Disponible en **www.hormigonyacero.com**
https://doi.org/10.33586/hya.2026.4128

A Levels-of-Approximation Unified Mechanical Model for the Shear Strength of Slender and Short Reinforced and Prestressed Concrete Beams with Steel, FRP, or Fiber Reinforced Concrete

Un modelo mecánico unificado de niveles de aproximación para la resistencia a cortante de vigas esbeltas y cortas de hormigón armado y pretensado con acero, FRP o hormigón reforzado con fibras

Antoni Cladera[a,*], Eva Oller[b], Carlos Ribas[a], Juan Murcia-Delso[b], Noemí Duarte[b], Jesús Miguel Bairán[b]

[a] *Department of Industrial Engineering and Construction. Universitat de les Illes Balears, Spain.*
[b] *Department of Civil and Environmental Engineering. Universitat Politècnica de Catalunya, Spain.*

Recibido el 8 de mayo de 2025; revisado el 20 de diciembre de 2025, aceptado el 28 de enero de 2026

ABSTRACT

This paper presents a Levels-of-Approximation (LoA) unified mechanical model for the shear strength of slender and non-slender reinforced and prestressed concrete beams, with rectangular, T- or I-shaped sections. It applies to members reinforced with steel or fiber-reinforced polymer (FRP) bars, or fiber-reinforced concrete (FRC). Derived from the Multi-Action Shear Model (MASM), the model integrates the key shear transfer actions, including shear carried by the compression chord, residual tensile stresses across the critical crack, dowel action of longitudinal reinforcement and contributions from stirrups, if present.

Structured within the LoA framework, the model offers increasing complexity and accuracy for various structural design and assessment scenarios, from preliminary design (LoA 0) to detailed assessment (LoA III). Its adaptability is demonstrated through different extensions, including fatigue for RC beams without stirrups. The model is validated using 2,714 test results from 14 experimental databases, showing consistent predictions with reduced scatter, especially at higher LoAs.

This unified mechanical model provides a robust tool for both the design and assessment of structural concrete elements, offering a systematic approach to integrate advanced mechanical understanding with practical engineering needs.

KEYWORDS: Shear strength, structural concrete, mechanical model, reinforced concrete, prestressed concrete, FRP, SFRC, fatigue.

RESUMEN

Este artículo presenta un modelo mecánico unificado, estructurado bajo la metodología de Niveles de Aproximación (LoA, por sus siglas en inglés), para estimar la resistencia a cortante de vigas esbeltas y no esbeltas de hormigón armado y pretensado, con secciones transversales rectangulares, en T o en I. El modelo es válido para elementos reforzados con barras de acero o de polímeros reforzados con fibra (FRP), así como para hormigones reforzados con fibras (FRC). Derivado del *Multi-Action Shear Model* (MASM), el modelo integra los principales mecanismos de transferencia del

esfuerzo cortante, incluyendo la contribución de la cabeza comprimida, las tensiones residuales de tracción a través de la fisura crítica, el efecto pasador de la armadura longitudinal y la contribución de la armadura transversal, si la hubiera.

El modelo, estructurado en el marco de los Niveles de Aproximación, ofrece una complejidad y precisión crecientes para distintos escenarios de proyecto y evaluación estructural, desde el diseño preliminar (LoA 0) hasta la evaluación detallada (LoA III). Su adaptabilidad se demuestra mediante diversas extensiones, incluyendo el análisis a fatiga en vigas de hormigón armado sin estribos. La validación se ha realizado con 2.714 resultados experimentales procedentes de 14 bases de datos, mostrando predicciones consistentes y con baja dispersión, especialmente en los niveles más elevados de aproximación.

Este modelo mecánico unificado constituye una herramienta robusta tanto para el proyecto como para la evaluación de elementos estructurales de hormigón, proporcionando un enfoque sistemático que integra un conocimiento mecánico avanzado con las necesidades prácticas de la ingeniería.

PALABRAS CLAVE: Resistencia a cortante, hormigón estructural, modelo mecánico, hormigón reforzado, hormigón pretensado, FRP, SFRC, fatiga.

* Persona de contacto / *Corresponding author*:
Correo-e / *e-mail*: antoni.cladera@uib.es (Antoni Cladera)

How to cite this article: Cladera, A., Oller, E., Ribas, C., Murcia, J., Duarte, N., Bairán, J.M. (2026). A Levels-of-Approximation Unified Mechanical Model for the Shear Strength of Slender and Short Reinforced and Prestressed Concrete Beams with Steel, FRP, or Fiber Reinforced Concrete. *Hormigón y Acero*. 77(308):71-92. https://doi.org/10.33586/hya.2026.4128

1. INTRODUCTION

The long-standing debate on the shear strength of reinforced concrete (RC) members dates back to the earliest research in this field. As early as 1907, Mörsch identified three fundamental shear transfer actions or resisting mechanisms [1]: 1) shear stresses in the compression zone, 2) dowel action in the longitudinal reinforcement, and 3) tensile forces in the web reinforcement, if present. Faber introduced the arch effect as another crucial mechanism in a series of superb papers published in 1916 [2]. However, it was not until 1966 that Fenwick and Paulay [3,4], through ad-hoc experiments, systematically analyzed the principal mechanisms of shear resistance in RC beams and were the first to quantify their contributions experimentally. Their pioneering work also incorporated aggregate interlock across cracks and marked the first estimation of shear stress attributable to this mechanism. These findings became a foundational step for further research and were incorporated into the ACI-ASCE recommendations in 1973 [5].

Subsequent studies focused on quantifying the contributions of each shear transfer mechanism, particularly aggregate interlock [6–8]. Prof. Fritz Leonhardt, in his famous keynote address, highlighted that ultimate shear strength is influenced by more than 20 parameters [9]. Since then, researchers have developed increasingly sophisticated models to account for many of these factors, while practical design codes require simplifications. As Prof. Paul E. Regan observed in 1993 [10], simplifying the problem often involves neglecting secondary factors, but what is secondary in one case may be primary in another. An example of this balance is the ACI-318-19 design formula for shear strength [11], which is derived from six models based on different assumptions [12–17]. Of these, two prioritize aggregate interlock as the dominant mechanism [14,15], while the remaining four focus on shear stresses transferred by the compression zone.

In recent years, Campana et al. [18] proposed a novel methodology for evaluating shear transfer mechanisms during testing, combining detailed crack pattern analysis and crack kinematics. This approach allowed researchers to track the evolution of shear-transfer actions during different loading phases. Cavagnis et al. [19,20] and Huber et al. [21,22] enhanced this methodology by incorporating Digital Image Correlation techniques and advanced models of aggregate interlock. Cavagnis et al. demonstrated that the relative contributions of shear-transfer actions vary with beam geometry and loading conditions. For slender beams ($a/d > 2.5$), aggregate interlock predominates, whereas for short beams ($a/d < 2.5$), direct strut-and-tie mechanisms govern the behavior. This transition occurs at the vertex of the so-called Kani valley [23], where the dominant shear mechanism shifts with the slenderness ratio.

Recently, Montoya et al. [24] used the Digital Image Correlation (DIC) technique to measure the sliding and opening of cracks in six RC beams without transversal reinforcement. This enabled using the Walraven model to compute the stresses along cracks, and estimated a reduced contribution of the aggregate interlock across the shear crack in the web, until approximately 90%–98% of the total shear capacity according to six tests on RC beams without stirrups (Fig. 1b). At this loading level, a second, more horizontal branch of the critical shear crack forms (Fig. 1c) inside the compression chord, accompanied by significant sliding resulting in higher levels of shear stresses. These observations highlight a complementary relationship, rather than a contradiction, between models based on shear transferred through the compression chord [25–27] and those prioritizing aggregate interlock [28,29], including the branch of the crack in the compression chord.

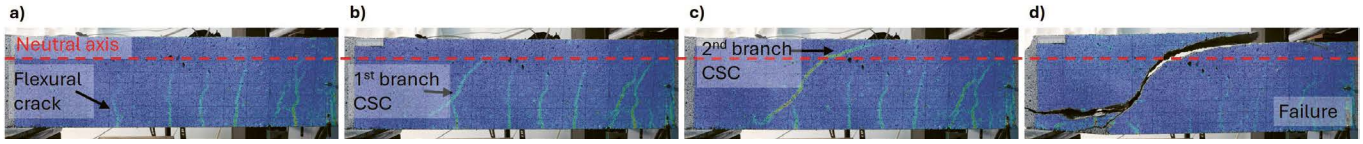

Figure 1. Crack pattern evolution in a RC beam, without stirrups, failing on shear.

A different methodology was employed by Bairán et al. [30], using optimized strut-and-tie models with concrete ties to understand shear transfer actions in RC beams without stirrups. This model considers stress transfer capacity across cracks by accounting for the inclination between the stress field and crack kinematics (opening and sliding). An experimental case study demonstrated that different shear-resisting actions dominate in different regions of the beam. For instance, aggregate interlock effectively transfers stresses in zones with near-vertical cracks. However, in areas with smaller bending moments and more inclined cracks, the stress components in the crack plane primarily induce direct tension with limited shear in the crack plane. Consequently, aggregate interlock becomes insufficient to carry the full shear force, and failure is governed by the compression zone's capacity.

In this context, two research groups—from the *Universitat Politècnica de Catalunya* and the *Universitat de les Illes Balears*—led by Prof. Antonio Marí, sequentially developed a mechanically derived shear strength model between 2014 and 2016. The initial development of the model began with efforts to explain the shear strength in ULS of beam-and-block floors [31] and beams reinforced with fiber-reinforced polymer (FRP) bars [32,33]. In both cases, it was observed that shear transfer in the compression zone was the dominant mechanism: in the first case, due to the prominence of the compression zone relative to the web width, and in the second case, due to the large crack widths in the web caused by the low modulus of elasticity of the FRP bars.

Building on these specific cases and integrating different transfer actions, as will be summarized in the following section, the general shear-flexural strength mechanical model for the design and assessment of reinforced concrete beams was formulated. This was initially applied to beams with rectangular cross-sections [34], then extended to T- and I-shaped beams [35], and finally to prestressed concrete beams [36]. Collectively, these contributions formed what we termed the Multi-Action Shear Model (MASM). The particular case of beams subjected to distributed loads was addressed in [37].

As the MASM presented closed-form equations for each shear transfer action, the model was simplified into the Compression Chord Capacity Model (CCCM), with the main premise that the shear transferred across the uncracked compression chord was the principal transfer action [38]. This simplified model also served as the base for the version developed for the ACI 318-19 update [16].

These mechanical models were further extended to address specific cases, including the shear strength of non-slender reinforced concrete beams [39], steel fiber reinforced concrete (SFRC) beams without stirrups [40], and the shear fatigue strength of RC members without stirrups [41]. Other applications included corrosion-damaged RC beams [42] and their long-time shear strength prediction [43,44], and prestressed concrete beams with FRP tendons [45]. The model was even adapted for punching shear of slabs [46,47], among other cases [48–50] not discussed here for the sake of conciseness. Moreover, a detailed discussion on open questions on shear behavior of structural concrete and the answers provided by mechanical models was recently published by Prof. Marí [51].

The 21 references cited earlier represent the culmination of approximately 12 years of dedicated and dynamic research. While these contributions were not always developed in a strictly sequential or comprehensive manner, each played a vital role in advancing the overall understanding of the subject. To bring coherence and clarity, this paper brings together those valuable insights into a unified mechanical model, structured in a logical progression—from the most general formulations to the more commonly encountered specific applications. Additionally, the work embraces the Level-of-Approximation (LoA) framework introduced in the Model Code 2010 [52], reinforcing a consistent and practical approach to model development.

The LoA framework ensures that the refinement of a design model corresponds to the required level of detail in the calculation process—whether for preliminary design, detailed design, or structural assessment—and considers the importance of the structural element in question [53]. For preliminary design, quick estimations are prioritized, requiring minimal calculation effort. In contrast, the strength assessment of existing structures often requires sophisticated models for accurate capacity evaluation, as decisions regarding reinforcement, rehabilitation, or demolition can carry substantial financial, social, and environmental implications. Accordingly, the complexity and effort involved in the design process increase with the LoA.

To maintain consistency across all LoAs, a unified physical model serves as the foundation, with conservative simplifications applied as the design complexity decreases. In this paper, the most refined model, corresponding to LoA III, is based on the Multi-Action Shear Model (MASM). From this formulation, the Compression Chord Capacity Model (CCCM) is transparently derived and proposed as LoA II. Further simplifications, tailored primarily for the design of new structures, constitute LoA I. Additionally, a preliminary design approach, referred to as LoA 0, is also discussed. This framework ensures coherent outcomes across different LoAs, with naturally more conservative results associated with lower levels of approximation, suitable for situations where data may be incomplete or imprecise.

This paper will present the LoAs in the logical sequence of their derivation (LoA III → II → I/0) although the intended use would be in the reverse order (LoA 0/I → II → III).

The key contribution of this work is the integration of the MASM and CCCM within a unified Level-of-Approximation framework. To the authors' knowledge, this is probably the first unified model capable of addressing a broad range of cases involving the shear strength of slender and short reinforced and prestressed concrete beams, with or without stirrups, considering

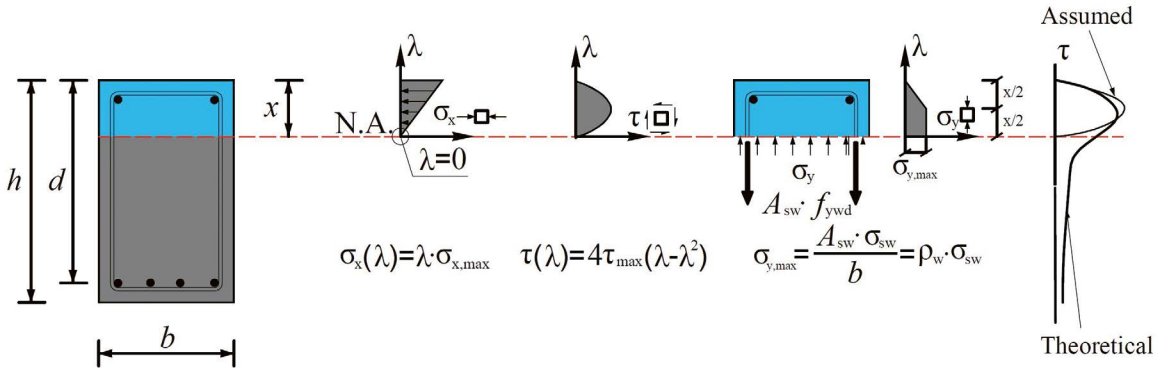

Figure 2. Considered distributions of stresses at the un-cracked concrete chord.

TABLE 1.
Summary of the equation for the LoA III: MASM

	Main expressions	
Shear strength	$V_{Rd} = V_{cu}+V_{su} \le V_{Rd,max}$	(1)
Concrete contribution	$V_{cu} = (v_c + v_w + v_l)\,\frac{f_{ct}}{\gamma_v}\cdot b\cdot d$	(2)
Shear reinforcement contribution	$V_{su} = (d_s-x)\,cot\theta\,\frac{A_{sw}}{s} f_{ywd}$	(3a)
	$V_s = (d_s-x)\,cot\theta\,\frac{A_{sw}}{s}\frac{f_{ywd}}{f_{ct}b\cdot d}$	(3b)
Maximum shear strength (strut crushing)	$V_{Rd,max} = \alpha_{cw}\, b_w\, z v_1\, f_{cd}\,\frac{cot\theta}{1+cot^2\theta}$	(4)
Contributing component	***Dimensionless expressions***	
Compression chord	$v_c = \zeta\left\{\left(0.70 + 0.18K_T + \left(0.20+0.50\,\frac{b}{b_w}\right)v_s\right)\,\frac{x}{d} + 0.02K_T\right\}\frac{b_{v,eff}}{b}K_p$	(5)
Cracked concrete web	$v_w = 167\,\frac{f_{ct}}{E_{cm}}\,\frac{b_w}{b}\left(1+\frac{2\cdot G_f\cdot E_{cm}}{f_{ct}^2\cdot d_0}\right)$	(6)
Longitudinal reinforcement (dowel effect)	$if\ \ v_s > 0 \rightarrow v_l = 0.23\,\frac{\alpha_e\cdot\rho_{l,b}}{1-x/d}$	(7a)
	$if\ \ v_s > 0 \rightarrow v_l = 0$	(7b)
Factors	***Expressions***	
Relative neutral axis depth	$\frac{x}{d} = \frac{x_0}{d} = \alpha_e\,\rho_{l,b}\left(-1+\sqrt{1+\frac{2}{\alpha_e\cdot\rho_{l,b}}}\right)$	(8a)
	$N_{Ed} > 0\ \ or\ P \rightarrow \frac{x}{d} = \frac{x_0}{d} + \Delta_{x/d} \le \frac{h}{d}$	(8b)
	$\Delta_{x/d} = \left(\frac{h}{d} - \frac{x_0}{d}\right)\left(\frac{h}{d}\right)\frac{\sigma_{cp}}{\sigma_{cp}+f_{ct}}$	(8c)
Effective flange width	$if\ x \le h_f \ \rightarrow\ b_{v,eff} = b_v = b_w + 2h_f \le b$	(9a)
	$if\ x > h_f \ \rightarrow\ b_{v,eff} = b_w + (b_v - b_w)\left(\frac{h_f}{x}\right)^{3/2}$	(9b)
Critical crack inclination	$cot\,\theta = \frac{0.85\,d_s}{(d_s-x)} \le 2.5$	(10)
Size and slenderness effect	$\zeta = \frac{2}{\sqrt{1+\frac{d_0}{200}}}\left(\frac{d}{a}\right)^{0.2}$	(11)
Parameter related to M_{cr} in T cross-section	$K_T = 0.1 + 0.9\,\frac{b_w}{b} + 2.5\,\frac{h_{f,tens}}{h}\left(\frac{b_{tens}-b_w}{b}\right)$	(12)
Parameter related to M_{cr} in prestressed members	$K_p = 1 + 0.3\,\frac{P\,cos\delta_p\,y_t}{f_{ct}\,bd^2}$	(13)

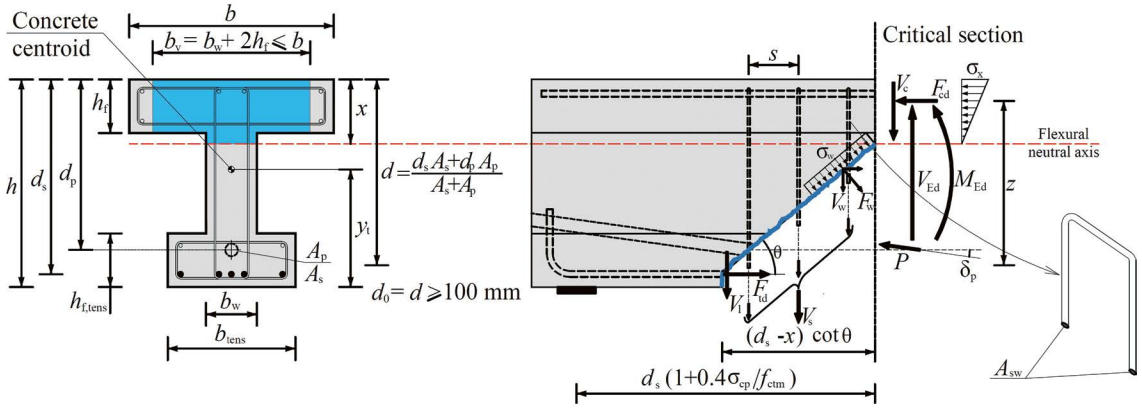

Figure 3. Graphical summary of the LoA III (MASM) with the definition of the basic parameters.

rectangular, T- or I-cross sections, with steel reinforcement, FRP reinforcement, or fiber-reinforced concrete. The extensions presented in this paper are primarily based on works previously published by the authors in separate contributions, which are here systematically compiled and adapted to ensure full internal consistency and practical applicability within the LoA framework, particularly at LoA II. This reorganization allows the different extensions to be applied in a homogeneous manner, providing a balanced compromise between mechanical accuracy and simplicity. In addition, in the specific case of beams internally reinforced with FRP bars—one of the earliest applications that motivated the development of the underlying mechanical model—the simplified formulation proposed at LoA II constitutes a new contribution, offering a more straightforward and fully integrated approach within the unified framework, now accounting for the successive developments of the general model.

2. BRIEF INTRODUCTION TO THE DERIVATION OF THE MULTI-ACTION SHEAR MODEL

The primary assumption of the Multi-Action Shear Model (MASM), supported by the empirical observations of many researchers [25,54,55], is that once the second branch of the critical crack develops, the load capacity does not significantly increase, as the softening of concrete in the compression zone begins.

Linking the onset of shear failure to the propagation of the second branch of the critical crack simplifies the problem significantly. This approach enables the formulation of a failure criterion based on concrete stresses in the compression chord, using Kupfer's biaxial failure envelope [56]. This criterion relies on the compressive and tensile strengths of concrete, parameters that exhibit less variability compared to those required in kinematic failure models.

In essence, the MASM assumes that the uncracked concrete in flexure experiences a multiaxial state of principal stresses (σ_1, σ_2), induced by the combined effects of shear force (τ), longitudinal bending stresses (σ_x), and vertical stresses (σ_y) from local effects (Figure 2), which collectively enhance the shear strength of the uncracked concrete. Building upon this assumption and applying classic mechanics principles, the MASM derives explicit equations (detailed in Section 3) for four shear transfer actions: shear transferred by the compression zone, shear transferred across the critical crack due to residual tensile stresses, shear transferred by dowel action of the longitudinal reinforcement, and shear transferred by the stirrups, if they exist. These actions are interdependent. For instance, the confinement stresses in the uncracked concrete, induced by stirrups, are accounted for when evaluating the shear contribution from the uncracked concrete, or the dowel effect is considered negligible if there are not stirrups. A comprehensive derivation of the MASM can be found in [29].

3. LEVEL OF APPROXIMATION III: THE MULTI-ACTION SHEAR MODEL (MASM)

Table 1, presenting Eqs. (1)-(13) and Figure 3, shows all the equations and factors needed to compute the shear strength of a reinforced or prestressed concrete member, with or without stirrups, with rectangular, T- or I-shaped cross-section. The key aspects and distinct features of this model will be highlighted

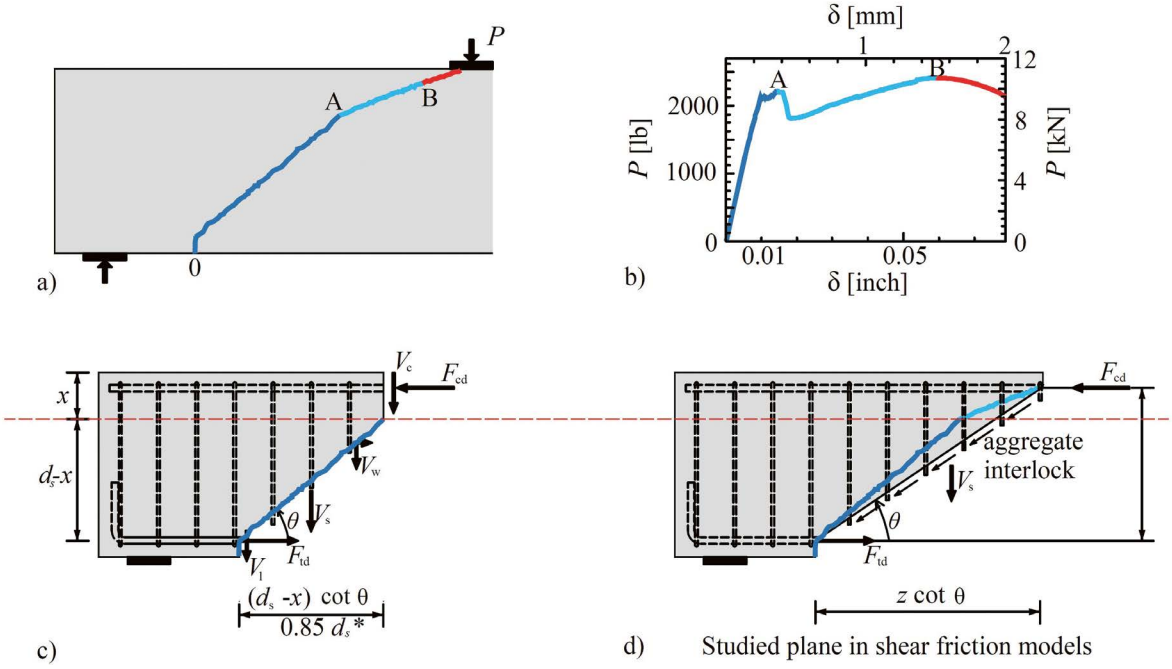

Figure 4. Qualitative scheme of crack propagation: a) crack trajectory [54]; b) load-displacement curve [54]; c) critical crack in MASM and simplified models; d) studied plane in shear friction models vs. the critical crack in MASM.

in the following subsections. Refer to the Notations section for the definition of the different parameters involved.

3.1. Relative neutral axis depth, x/d

The ratio of the neutral axis depth to the effective depth, x/d, is the key dimensionless parameter governing shear strength in the proposed model. For RC members, this parameter is determined by Eq. (8a), while for PC or RC members subjected to compressive axial loads, it is given by Eqs. (8b) and (8c).

As previously discussed and illustrated in Fig. 1, the shear critical crack (SCC) evolves from an initial flexural crack and develops in two distinct stages. This two-phase behavior has also been observed by other researchers during tests on notched specimens specifically designed to investigate mixed-mode crack propagation in reinforced concrete (see Figs. 4a and 4b) [54]. From Fig. 4, it becomes evident that internal forces may redistribute between stages 0-A and A-B of the load-displacement curve.

The MASM and its simplified models (Fig. 4c) focus on the crack stage corresponding to Point A in Fig. 4a, representing the onset of critical crack propagation. In contrast, models based on aggregate interlock or shear friction are typically concerned with the fully developed crack (Fig. 4d), where shear friction stresses are related to flexural strains, assessed at the level of the longitudinal reinforcement or at a specified depth in the web.

For quick estimations and to grasp the order of magnitude, typical x/d values as a function of the tensile reinforcement ratio, $\rho_{l,b}$, are $x/d \approx 0.20$ for lightly RC beams, $x/d \approx 0.25$ for conventionally RC beams, or $x/d \gtrapprox 0.35$ for heavily RC beams.

For PC members, Eqs. (8b) and (8c), derived in [36], apply. Notably, these formulas are straightforward and applicable to both prestressed members and members subjected to compressive loads. The increase in the neutral axis depth depends on the ratio $\frac{\sigma_{cp}}{\sigma_{cp}+f_{ct}}$, rather than solely on σ_{cp}.

The MASM (LoA III) has not been validated for members under tensile loads. However, the CCCM (LoA II) has been validated in such cases, as will be detailed in Section 4. For these scenarios, it is necessary to account for the concomitant bending moment, M_u, in the design sections [38].

3.2. Size and slenderness effect

The brittle nature of failure that occurs when the second branch of the critical crack propagates demands considering the size effect, which depends on the dimensions of the concrete region subjected to compressive and tensile stresses. To account for this, a combined size and slenderness factor is defined in Eq. (11). This factor integrates the size effect term proposed by the ACI Committee 446 [57] (first term in the equation) with a slenderness-dependent term, based on the shear span-to depth ratio, a/d, derived from empirical studies using genetic programming [58,59]. These studies demonstrated that the term $d/a^{0.21}$, simplified to $d/a^{0.2}$, accurately predicts the influence of slenderness. For accurate calculations in continuous beams or beams with distributed loads, it is recommended to refer to the definition of the shear span, a.

This integration represents a significant advancement, as it unifies the MASM and CCCM formulations while grounding the size effect treatment in a robust theoretical framework. In the original MASM formulation, an empirical factor proposed by other authors was adopted [25]. The updated approach is theoretically consistent, as the failure in the MASM is fully coherent with the failure explained by the fracture mechanics-based models [17,54,55].

3.3. Effective compression flange width

The influence of compression flanges on shear transfer mechanisms was thoroughly analyzed during the derivation of the MASM for T- and I-shaped beams [35]. However, to make the model more practical for everyday engineering applications, these effects were simplified into more compact expressions. In the MASM, the contribution of the compression flanges to shear strength is accounted for through an effective flange width, defined by Eqs. (9a) and (9b). This effective width depends on the section geometry and on the neutral axis depth. For further details, refer to the figure included in Table 1.

It should be noted that for rectangular beams, the effective flange width corresponds to the section width ($b = b_{v,eff} = b_w$). For L-shaped sections with a compression flange, the term $2h_f$ of Eq. (9a) is replaced by h_f, which represents the thickness of the compression flange.

3.4. Critical crack inclination

The inclination of the critical crack is a key parameter in evaluating shear strength, as it determines where the critical crack intersects the compression zone and affects the contribution of shear reinforcement, which depends on the number of stirrups intersecting the first branch of the critical crack. Based on experimental observations reported by the authors in [35], the horizontal projection of the first branch of the critical flexural-shear crack is assumed to be $0.85d_s$ (see Fig. 4c). This assumption corresponds to the crack inclination defined in Eq. (10).

Crack inclination is influenced by both the longitudinal and transverse reinforcement ratios, ρ_l and ρ_w, as these factors affect the strain distribution. However, longitudinal reinforcement has been found to have a more significant impact on crack inclination, as observed by other researchers [29,32]. For this reason, the MASM simplifies the analysis by focusing on the longitudinal reinforcement through its relationship with the neutral axis depth. This approach ensures the model remains straightforward and non-iterative, making it suitable for both design and assessment purposes.

As the longitudinal reinforcement ratio increases, the mean inclination angle of the critical crack decreases. This is consistent with the fact that for the same shear strain, the longitudinal tensile strain, ε_x, is lower when the longitudinal reinforcement ratio increases. For simplicity, the model assumes that the inclination angle of the critical crack is equal to the angle of the struts (θ), when verifying the maximum shear strength according to Eq. (4).

3.5. Position of the critical section and the critical point inside the compression chord

As the applied load increases, flexural cracks progressively develop with increasing bending moments. The critical crack is assumed to be the one closest to the zero bending moment point

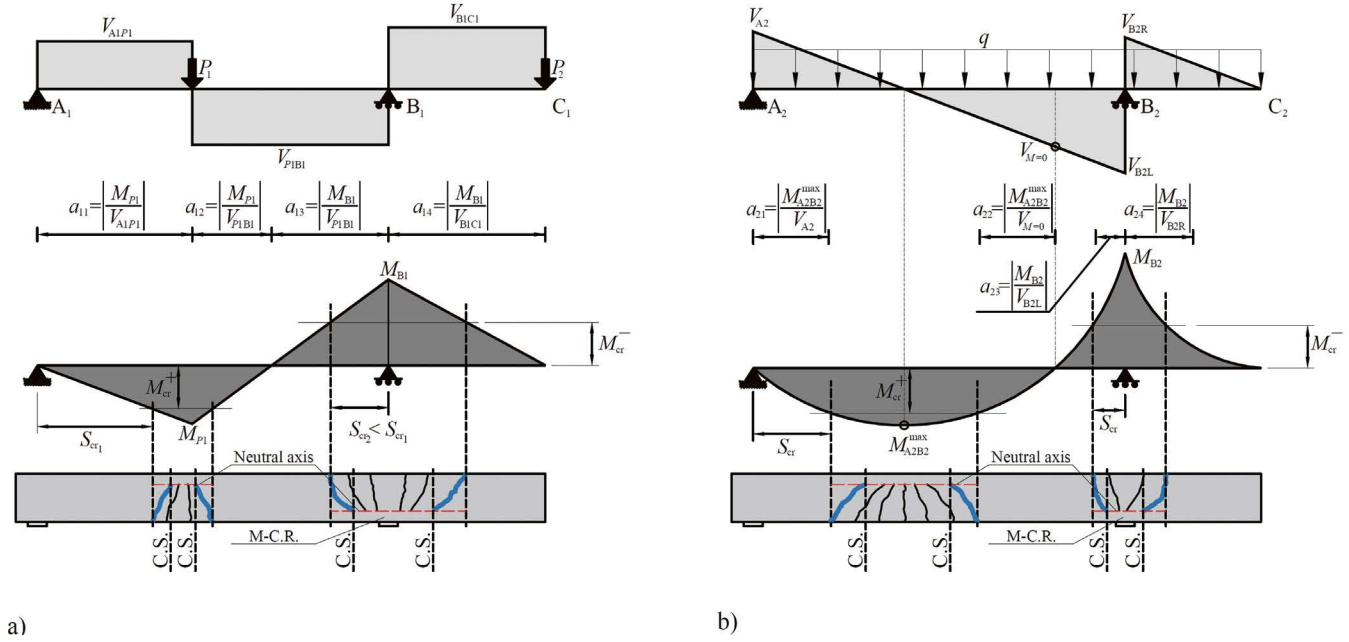

Figure 5. Location of critical section: a) Simply supported region and cantilever under concentrated loads; b) Simply supported region and cantilever under distributed loads.

Note: C.S.: critical section; M-C.R: multi-compressed region.

(see Fig. 1), initiating at the location where the bending moment diagram at failure reaches the cracking moment of the cross-section. The critical section, where equilibrium equations were set in the derivation of the model, is located at the point where this critical crack intersects the neutral axis depth (see Fig. 5).

Based on these considerations, and on the vertical crack horizonal projection defined in Section 3.4, the distance between the zero bending moment point and the initiation of the critical crack is $s_{cr} = M_{cr}/V_u$, and the critical section is positioned at $s_u = s_{cr} + 0.85d_s$. Typically, this distance slightly exceeds d_s, which is why, for design purposes, ds is used as the location to verify the shear strength of RC members.

In PC members, the higher cracking moment shifts the critical crack farther from the zero bending moment point compared to RC members. To address this, it is proposed to verify the shear strength at a section located at a distance $d_s(1+ 0.4\sigma_{cp}/f_{cm})$. The increased cracking moment in prestressed sections is incorporated into the mechanical model through the strength factor K_p (Eq. 13 in Table 1), while the influence of the compression or tensile flanges on the cracking loads is accounted for by factor K_T (Eq. 12). For RC beams without axial loads and rectangular cross-sections, $K_p = K_T = 1$.

The critical point within the compression chord, where failure is expected to initiate, corresponds to the location of maximum damage. Its position depends on the distributions of normal and shear stresses along the uncracked concrete chord. While this specific point is not directly used in the application of the MASM, it is of theoretical interest. Studies conducted by the authors [32] indicate that, assuming linear and parabolic distributions for the normal and shear stresses, respectively, the critical point is located at a distance of approximately $y \approx 0.425x$ from the neutral axis.

4. LEVEL OF APPROXIMATION II: THE COMPRESSION CHORD CAPACITY MODEL (CCCM)

The derivation of the CCCM equations (Table 2, Eqs. (14)-(21) and Figure 6) from MASM is detailed in Appendix A. To simplify the application of LoA II, the complete set of equations is provided, though many parameters (Eqs. 18a, 18b, 18c, 19a, 19b, 20 and 21) remain as defined for MASM in Table 1.

For RC beams, Eq. (18a) introduces a simplified expression for the relative neutral axis depth (term on the right), which shows good accuracy as demonstrated in [38]. A simplification for the expression of maximum shear strength is proposed in Eq. (17), with its derivation detailed in Annex A3.

The reduction of neutral axis depth for RC beams under tensile axial loads is addressed by Eq. (18d). While this approach simplifies the problem, the model still performs well, as shown in Section 7 and [60].

5. LEVEL OF APPROXIMATION I AND 0

In cases where lower computational effort is sufficient, LoA I provides a simplified alternative. Derived from LoA II (CCCM) as detailed in Appendix B, this approach assumes all cross-sections are rectangular, disregarding the beneficial effects of compression flanges. The model, outlined in Table 3 (Eqs. (22)-(28) and Figure 7), is applicable to RC and PC

TABLE 2.
Summary of the equations for the LoA II: CCCM

	Main expressions	
Shear strength	$V_{Rd} = V_{cu} + V_{su} \leq V_{Rd,max}$	(14)
Concrete contribution	$V_{cu} = \zeta \frac{x}{d} \frac{f_{ct}}{\gamma_v} b_{v,eff}\, d \geq V_{cu,min}$	(15)
	$V_{cu,min} = 0.18\left\{\zeta + \frac{100}{d_0}\right\} \frac{f_{ct}}{\gamma_v}\, b_w d$	(15a)
Shear reinforcement contribution	$V_{su} = 1.4\,(d_s - x)\, cot\theta \frac{A_{sw}}{s} f_{ywd}$	(16)
Maximum shear strength (strut crushing)	$V_{Rd,max} = \alpha_{cw}\, b_w\, z \nu_1 f_{cd} \frac{cot\theta}{1+cot^2\theta} \approx 0.225\, f_{cd}\, b_w d$	(17)
Factors	***Expressions***	
Relative neutral axis depth	$\frac{x}{d} = \frac{x_0}{d} = \alpha_e \rho_{l,b} \left(-1 + \sqrt{1 + \frac{2}{\alpha_e \cdot \rho_{l,b}}}\right) \approx 0.75\,(\alpha_e\, \rho_{l,b})^{1/3}$	(18a)
	$N_{Ed} \neq 0 \;\; or \;\; P \rightarrow 0 \leq \frac{x}{d} = \frac{x_0}{d} + \Delta_{x/d} \leq \frac{h}{d}$	(18b)
	$N_{Ed} > 0 \;\; or \;\; P \rightarrow \Delta_{x/d} = \left(\frac{h}{d} - \frac{x_0}{d}\right)\left(\frac{d}{h}\right) \frac{\sigma_{cp}}{\sigma_{cp}+f_{ct}} > 0$	(18c)
	$N_{Ed} < 0 \qquad \rightarrow \Delta_{x/d} = 0.1 \frac{N_{Ed}}{M_{Ed}} \frac{d_s}{d} < 0$	(18d)
Effective flange width	$if\; x \leq h_f \;\; \rightarrow \;\; b_{v,eff} = b_v = b_w + 2h_f \leq b$	(19a)
	$if\; x > h_f \;\; \rightarrow \;\; b_{v,eff} = b_w + (b_v - b_w)\left(\frac{h_f}{x}\right)^{3/2}$	(19b)
Critical crack inclination	$cot\,\theta = \frac{0.85\, d_s}{(d_s - x)} \leq 2.5$	(20)
Size and slenderness effect	$\zeta = \frac{2}{\sqrt{1 + \frac{d_0}{200}}} \left(\frac{d}{a}\right)^{0.2}$	(21)

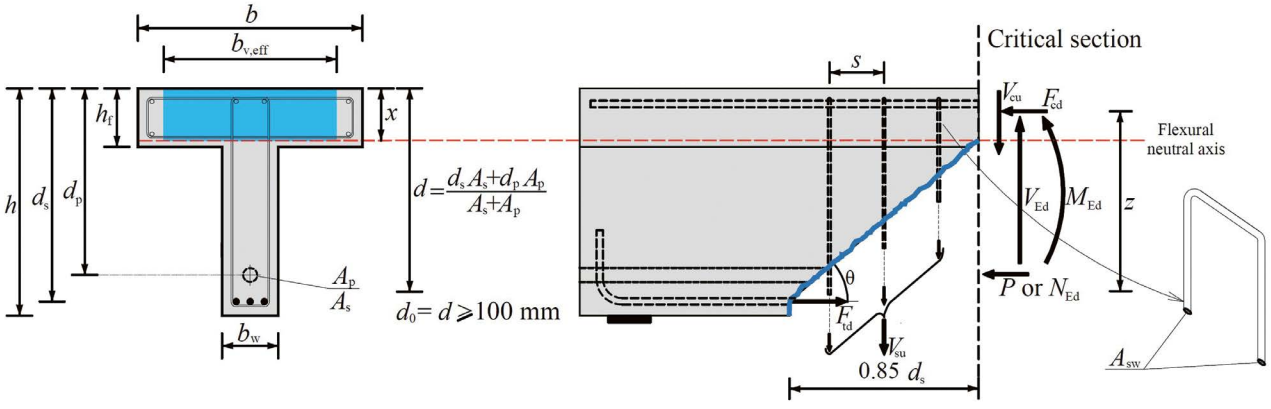

Figure 6. Graphical summary of the LoA II (CCCM) with the definition of the basic parameters.

elements with or without stirrups but does not account for tensile axial forces.

In the most complex case—a PC beam with an I-cross section and stirrups—LoA I requires only 7 equations and 12 variables, compared to the 18 equations and 21 variables used in LoA III (MASM, see Table 1). LoA II (CCCM) offers an intermediate level of complexity.

Eq. (24) defines the lower-bound shear strength for members with low longitudinal reinforcement, making it independent of the longitudinal reinforcement ratio. Due to its simplicity, this equation is designated as LoA 0. Note that within the brackets of Eq. (24), two size effects are considered: the compression chord size effect (ζ', left term) and the size effect due to the residual tensile stress transferred through the critical shear crack ($100/d_0$, right term).

6. UNCRACKED REGIONS IN BENDING

In highly prestressed, simply supported concrete beams—such as certain T- or I-shaped beams with minimal or no shear reinforcement—flexural cracking near the supports is often absent, even under significant loading. In these regions, the thin beam web experiences high shear stresses from the applied shear force, combined with compressive normal stresses induced by prestressing. This creates a biaxial stress state of compression and tension. When the principal stresses at the most critical point in the web exceed Kupfer's biaxial failure envelope [56], a diagonal crack forms across the entire beam height. Experimental evidence suggests that the cracking load in such cases is nearly identical to the ultimate load [61–63].

TABLE 3.
Summary of the Level of Approximation I procedure

	Main expressions	
Shear strength	$V_{Rd} = V_{cu} + V_{su} \leq V_{Rd,max}$	(22)
Concrete contribution	$V_{cu} = 1.35\zeta' \rho_{l,w}^{1/3} \frac{f_{ct}}{\gamma_v} b_w d(1+\Delta_{x/d}) \geq V_{cu,min}$	(23)
	$V_{cu,min} = 0.18\left\{\zeta' + \frac{100}{d_0}\right\} \frac{f_{ctm}}{\gamma_v} b_w d$	(24)
Shear reinforcement contribution	$V_{su} = 1.2 \frac{A_{sw}}{s} f_{ywd} d_s$	(25)
Maximum shear strength (strut crushing)	$V_{Rd,max} = 0.225 f_{cd} b_w d$	(26)
Factors	***Expressions***	
Prestressing effect	$N_{Ed} > 0 \ \ or \ P \rightarrow \Delta_{x/d} = \left(\frac{h}{d} - \frac{x_0}{d}\right)\left(\frac{d}{h}\right) \frac{\sigma_{cp}}{\sigma_{cp}+f_{ct}} > 0$	(27)
Size effect	$\zeta' = \frac{1.5}{\sqrt{1+\frac{d_0}{200}}}$	(28)

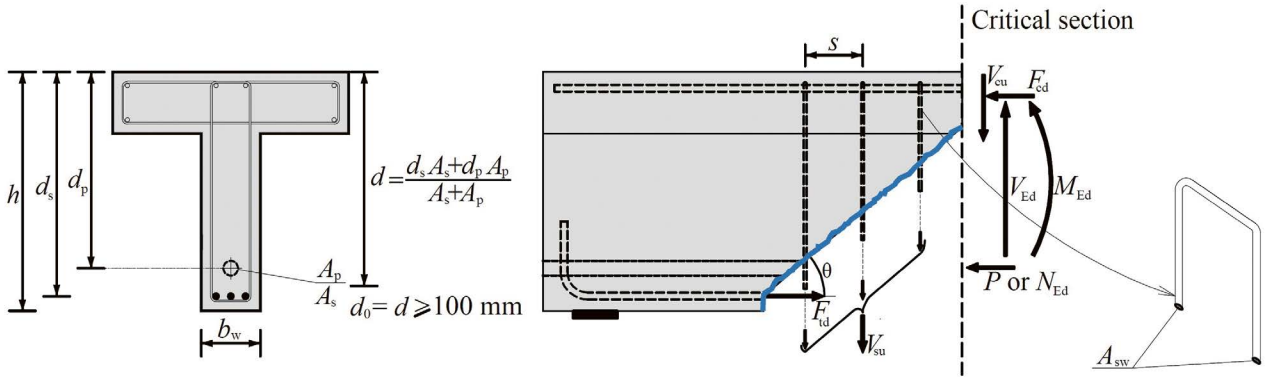

Figure 7. Graphical summary of the LoA I with the definition of the basic parameters.

As derived in [36], the shear strength under these conditions is given by Eq. (29):

$$V_{Rd} = \frac{I_c b_w}{S_c} 0.8 f_{ct} \sqrt{1+\alpha_1 \frac{\sigma_{cp}}{f_{ct}}} \tag{29}$$

The factor 0.8 in Eq. (29) accounts for the interaction between compressive and tensile stresses, as derived using Kupfer's failure envelope [36]. It is worth noting that some design codes omit this factor, which we consider a slightly unconservative approach.

For beams with transverse reinforcement, shear strength is calculated assuming the presence of flexural cracks. In such cases, the previously described levels of approximation (LoAs) should be used.

7. VALIDATION OF THE LOA 0, I, II AND III WITH EXPERIMENTAL DATABASES

The predictions of the defined Levels of Approximation (LoA) are validated against the ACI-DAfStb evaluation databases developed by ACI Subcommittee 445-D. These include RC beams without stirrups [64], RC beams with stirrups [65], PC beams without stirrups [66] and PC beams with stirrups [66]. Table 4 summarizes the primary statistics of the experimental-to-predicted strength ratios (V_{test}/V_{pred}).

For all comparisons in this paper, average concrete compressive strength and tensile steel strength values were used, with partial safety factors set to 1. For the concrete tensile strength, f_{ct}, and modulus of elasticity, E_c, the average values given in the Eurocode 2 of second generation [67] have been used (see Notations section for the exact definition).

Generally, as the LoA increases, both the mean V_{test}/V_{pred} ratio and its coefficient of variation (CoV) improve. LoA III demonstrates consistently low CoV across all databases, including the subsets of T-beams. In contrast, LoA I, which does not account for compression flanges, exhibits higher safety margins for T-beam subsets. Detailed comparisons with code-based methods are outside the scope of this paper but are available in [36,38]. Note that for PC beams without stirrups, each LoA is combined, depending on the cracking state for the predicted maximum load, with the shear strength for regions uncracked in bending.

Figure 8 illustrates the correlation between experimental results, V_{test}, and predictions for the four LoAs. The blue line represents perfect correlation, and dashed black lines indicate data trends, with R^2 values included. As observed, accuracy noticeably improves with higher LoA.

TABLE 4.
Comparison of tests results vs. predictions for different LoAs.

Database (or sub-database)	#	*LoA 0 ($V_{cu,min}$)*		*LoA I*		*LoA II*		*LoA III*	
		Mean	*CoV*	*Mean*	*CoV*	*Mean*	*CoV*	*Mean*	*CoV*
RC beams w/o stirrups	784	1.84	29.5%	1.27	22.9%	1.16	18.0%	1.03	17.8%
RC only T-beams w/o stirrups	64	2.19	35.6%	1.40	34.2%	1.09	22.2%	1.14	20.4%
RC beams with stirrups	170	1.53	22.4%	1.23	16.7%	1.14	14.2%	1.09	15.5%
RC only T-beams with stirrups	57	1.52	27.3%	1.34	15.1%	1.20	12.4%	1.21	12.7%
PC beams w/o stirrups	214	-	-	1.84	30.6%	1.21	22.8%	1.10	22.2%
PC only T-beams w/o stirrups	112	-	-	1.92	33.5%	1.21	21.8%	1.15	21.0%
PC beams with stirrups (115 with T-cross section)	117	-	-	1.48	23.2%	1.20	20.9%	1.10	14.4%

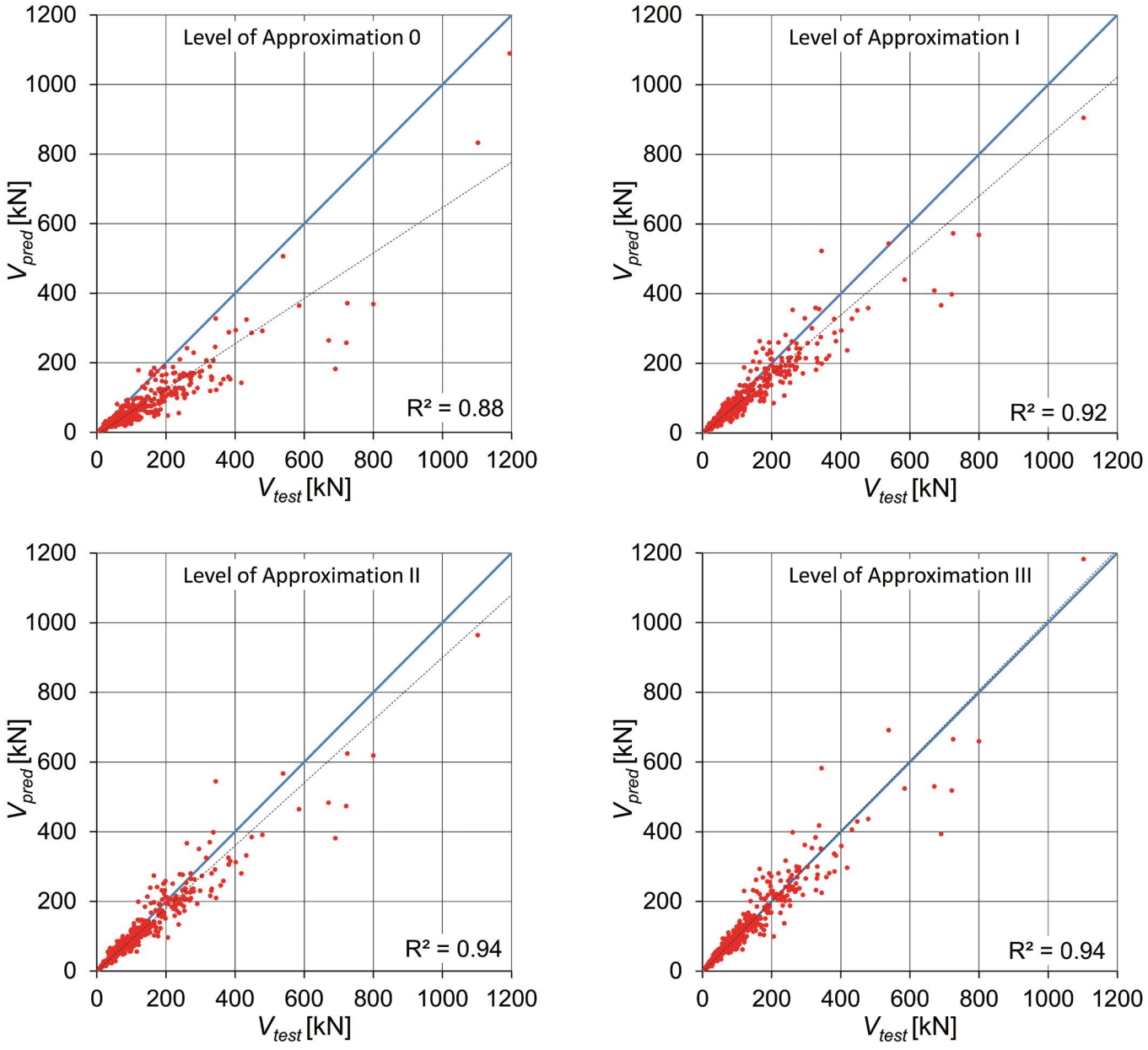

Fig. 8. Correlation between predictions and experimental results for RC beams w/o stirrups.

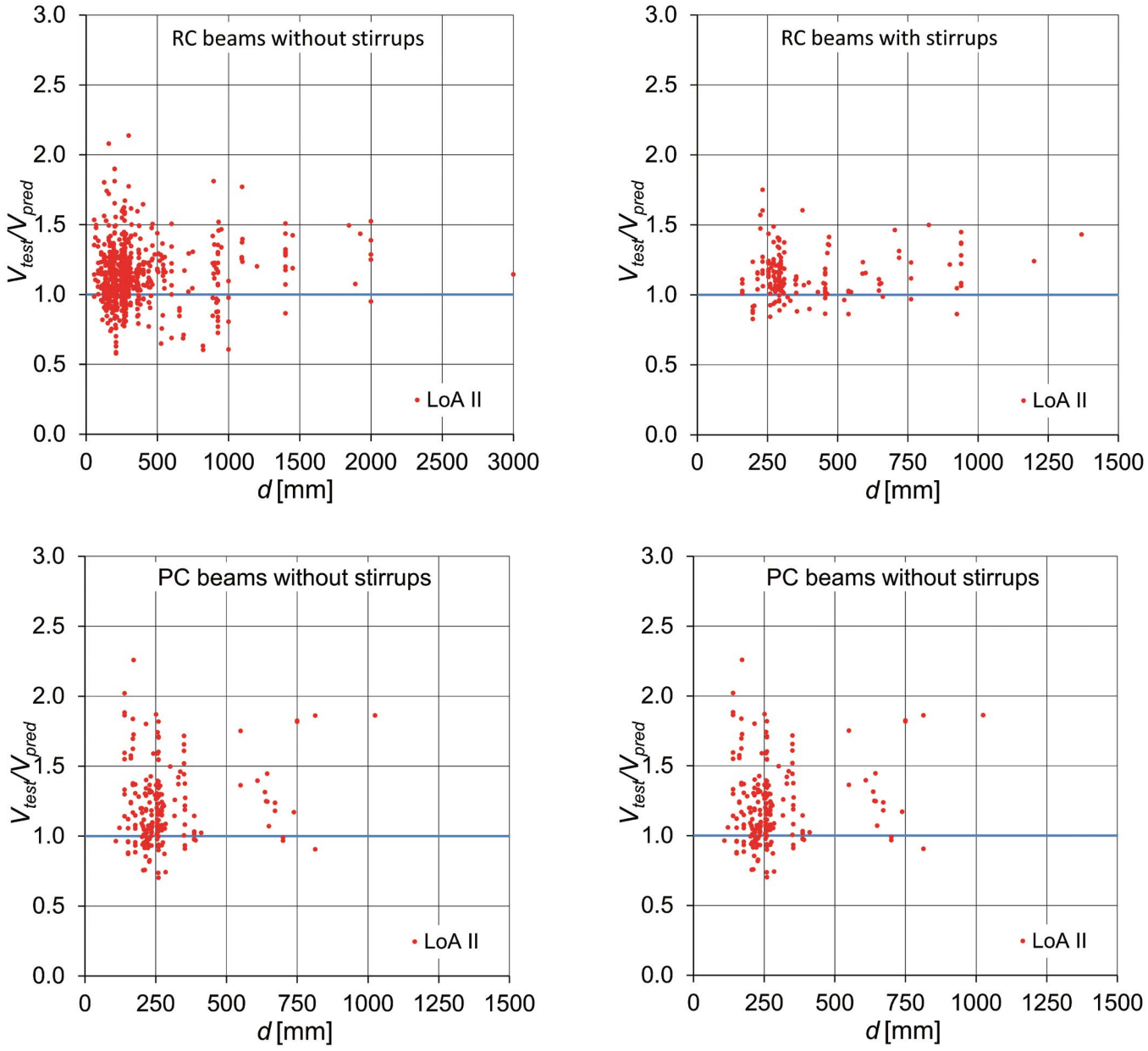

Figure 9. Correlation between LoA II and experimental results as a function of *d*.

Figure 9 shows the correlation between LoA II predictions and experimental results as a function of effective depth, *d*, for the four ACI-DAfStb databases. No significant trend against d is observed, confirming the appropriateness of the size effect factor.

It is worth noting that while the partial safety factor for concrete shear contribution is defined per Eurocode 2 (2nd generation) [67], this factor depends on the specific performance of the design model, as well as the uncertainties of its variables, so the direct interpolation to different models is, in general, not possible. Therefore, further reliability analyses are needed to calibrate the safety format of the presented LoAs for design purposes. As previously discussed, different shear mechanical models should be viewed as complementary rather than contradictory. For instance, for members with moderate or high amounts of shear reinforcement, variable-angle truss models based on plasticity offer a quick and practical design approach, particularly when torsion is present. For such members, a practical approach is to determine the maximum shear strength using either the models presented in this paper or variable-angle truss models based on plasticity, such as those included in the Eurocodes [67,68].

The LoA II (CCCM) incorporates the effect of axial tensile forces via Eq. (18d). To evaluate its predictive accuracy, two databases were analyzed. The first, from [69], includes 34 rectangular beams (a/d= 1.5–5.6) and 14 T-beams (a/d= 2.0). The second, from [70] contains 23 beams, some subjected to high axial tensile loads. Notably, Eurocode 2 predicts zero shear strength for 12 tests in this latter set, as noted in [60]. For the CCCM computations, the extension for non-slender beams presented in Section 8.1 has also been considered for beams with $a/d < 2.5$.

Figure 10 illustrates the V_{test}/V_{pred} correlations. For the first database (black and white circles), LoA II yields a mean ratio of 1.24 with a CoV of 21.1%. For the second (red circles), the mean ratio is 1.32 with a CoV of 13.8%. While these results are promising, it is crucial to note that under strong axial loads, $V_{cu,min}$ (Eq. (15b)) governs the prediction, as x/d may reduce to zero, rendering V_{cu} (Eq. (15a)) negligible. In such cases, the strong catenary effect could have had a significant impact on the shear strength, but this effect is outside the scope of this compact model. Careful application is advised in these scenarios.

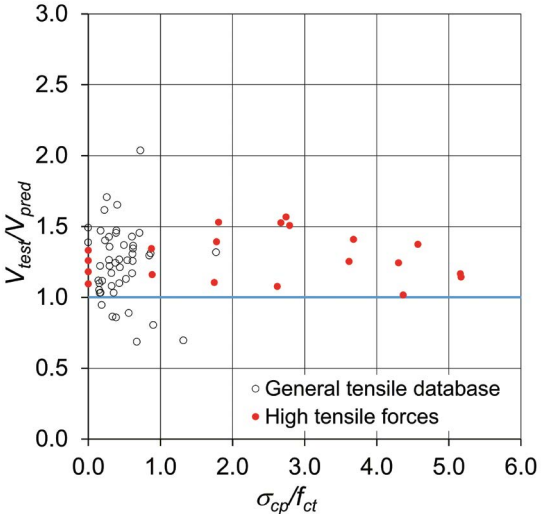

Figure 10. Correlation between LoA II predictions and experimental results as a function of non-dimensional tensile stress for the two databases.

8. MODEL EXTENSIONS

The following subsections present the key extensions developed by the authors. Each extension is summarized, followed by a brief comparison with the relevant databases for each case. For simplicity and computational efficiency, most extensions are based on LoA II, the Compression Chord Capacity Model.

8.1. Non-Slender Beams with and without stirrups

The shear strength of non-slender reinforced concrete beams, where $a/d \leq 2.5$, is enhanced due to arching action, as Kani [71] already showed in 1964. Existing shear design methods for such elements, including the strut-and-tie method (STM), show deviations from test results. The LoA II (CCCM), originally developed for slender beams, has been extended to non-slender beams. This extension incorporates the effects of non-planar strain distribution, the multi-compression stress state near the applied load, and the pre-determined position and inclination of the critical shear crack. The main equations for the extension are presented in Table 5 and Figure 11, with the full derivation provided in [39]. For any parameter or factor not listed in Table 5, the corresponding value from the CCCM (Table 2) should be used. This includes the relative neutral axis depth, x/d, for slender-beams.

The concrete contribution to shear strength is given by Eq. (30), which uses the shear strength for slender beams (dependent on x/d), multiplied by K_{ad}, a factor that accounts for the ratio between shear strengths in non-slender and slender beams (see Eq. 35).

To compute the contribution of the reinforcement to the shear strength, the relative neutral axis depth for non-slender beams must be determined. To account for the increase in neutral axis depth, a parabolic variation of x is assumed between a/d =2.5 (x_1=x, B-region) and a/d=0 (x_1=d), as seen in Eq. (36).

In non-slender beams, the critical shear crack develops straight and connecting the inner faces of the load to the support pads [72], with an inclination given by the shear-span-to-depth ratio, a/d, as seen in Eq. (37).

The web reinforcement contribution (Eq. 32) includes both vertical (stirrups) and horizontal reinforcement along the web. It is important to note that, in general, these reinforcements may not yield, and their stress contributions are considered using Eqs. (38a) and (38b).

To experimentally validate the proposed model for non-slender beams, the derived equations were used to predict the results of 486 tests. The datasets used for verification include: 222 tests on beams without web reinforcement [73], 178 tests on beams with vertical web reinforcement [74], and 86 tests on beams with horizontal and vertical web reinforcement [75]. The results are summarized in Table 6. Although some scatter is observed for RC beams without stirrups, the performance compares favorably to code procedures, as detailed in [39].

TABLE 6.
Comparison of tests results vs. predictions for non-slender beams.

Database	#	*LoA II*	
		Mean	*CoV*
RC beams w/o stirrups	222	1.47	29.5%
RC beams with vertical stirrups	178	1.19	19.4%
RC beams with vertical stirrups and longitudinal web reinforcement	86	1.37	22.1%

One fundamental contribution of the extension for non-slender beams is that it presents smooth continuity with LoA II for slender beams. This continuity is illustrated in Figure 12, which depicts results from Kani's renowned series of tests [23]. In these tests, key beam properties —such as width (154 mm), depth (610 mm), effective depth (539 mm), longitudinal reinforcement (ρ = 2.77 %, f_y =371.9 MPa), concrete and maximum aggregate size —were held relatively constant, while the shear-span-to-depth ratio, a/d, varied between 1 and 9. Because the beams were heavily reinforced longitudinally, flexural failures at midspan did not occur until a/d reached approximately 9 (beam 68 in Figure 12). The predictions for slender beams by LoA II (CCCM) are shown in red, while those for non-slender beams (a/d < 2.5) in blue. The figure highlights the satisfactory predictions and the consistency across both slender and non-slender beam cases.

TABLE 5.
Summary of the equations extended for non-slender beams

	Main expressions	
Shear strength	$V_{Rd} = V_{cu} + V_{su} \leq V_{Rd,max}$	(30)
Concrete contribution	$V_{cu} = \zeta \frac{x}{d} k_{ad} \frac{f_{ct}}{\gamma_v} b_{v,eff} d$	(31)
Web reinforcement contribution	$V_{su} = V_{swy} + V_{swx}$	(32)
Vertical web reinforcement	$V_{swy} = \frac{A_{swy}}{s_x} (d - x_1) \cot\theta \, \sigma_{swyd}$	(33)
Horizontal web reinforcement	$V_{swx} = 0.5 \frac{A_{swx}}{s_y} (d - x_1) \tan\theta \, \sigma_{swxd}$	(34)
Factors	***Expressions***	
Factor considering strength increase in non-slender beams	$k_{ad} = 1 + (2.5 - \frac{a}{d})^2$	(35)
Relative neutral axis depth	$\frac{x_1}{d} = \frac{x}{d} + (1 - \frac{x}{d})(1 - 0.4 \frac{a}{d})^2 \leq 1$	(36)
Critical crack inclination	$\cot\theta = \frac{a}{d} \geq 0.5$	(19a)
Stress at vertical and horizontal web reinforcement	$\sigma_{swy} = \frac{f_{ct} k_{ad}}{\rho_l} \frac{x_1}{d} \cot^3\theta \leq f_{ywd}$	(38a)
	$\sigma_{swx} = \frac{f_{ct} k_{ad}}{\rho_l} \frac{x_1}{d} \cot\theta \leq f_{ywd}$	(38b)

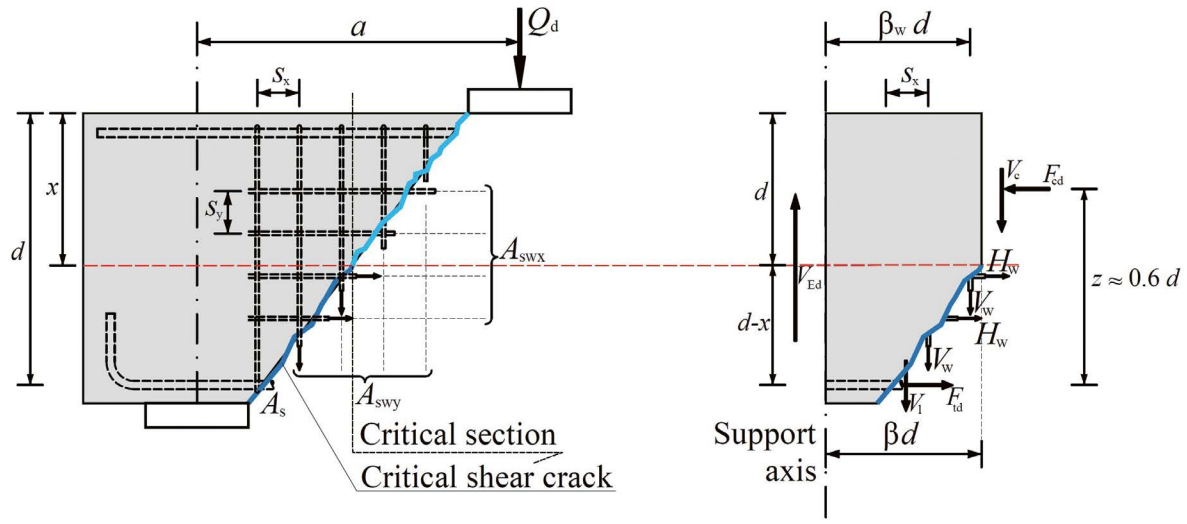

Figure 11. Graphical summary of the extension for non-slender beams.

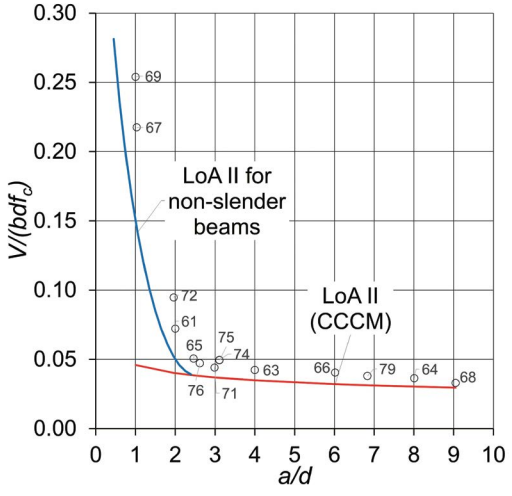

Figure 12. Predicted and observed strengths for Kani's RC beams [23].

8.2. Beams internally reinforced with FRP bars

For RC members reinforced internally with FRP bars—either longitudinal reinforcement alone or in combination with transverse FRP bars—crack widths tend to be larger than in beams reinforced with conventional steel bars [76]. This is due to the lower modulus of elasticity of FRP, which reduces aggregate interlock and increases the importance of shear transfer through the uncracked concrete chord. Notably, the development of MASM/CCCM models originated from this specific case [32,33].

For coherence with our other works, in this paper we propose using LoA II, i.e., the Compression Chord Capacity Model (Table 2), to also address this scenario. The modular ratio, α_e, should be computed considering the modulus of

elasticity of the FRP bars. Additionally, note that Eq. (15b), which defines $V_{c,min}$ is not applicable for RC beams reinforced internally with non-prestressed FRP bars. This equation assumed a significant contribution from shear transfer across the critical crack, v_w, which is less relevant in this context due to the material properties of FRP.

The contribution of the transversal FRP reinforcement, V_{fu}, is obtained using Eq. (16) but replacing the term f_{ywd} by σ_t, as defined in Eq. (39). This value accounts for two effects: 1) the tensile stress in FRP stirrups failing in the bent zone is assumed to be 45% of the ultimate strength of the straight portion of the bar, which corresponds to a mean value of the strength of the bent portion of the bar according to JSCE-97 [77] and ACI440.1R-15 [78] considering different ratios of the bent radius with respect to the bar diameter; and 2) σ_t represents the average stress of all stirrups crossing the critical crack, approximated as half of the stress in the most highly stressed stirrup.

$$\sigma_t = 0.225 \cdot f_{tu} \tag{39}$$

TABLE 7.
Comparison of tests results vs. predictions for beams with only FRP rebars.

Database (or sub-database)	#	*LoA II*	
		Mean	*CoV*
RC beams w/o stirrups	144	1.32	17.0%
RC beams with FRP stirrups	112	1.37	24.3%
PC beams with FRP tendons (with and w/o FRP stirrups)	55	1.13	25.8%

The LoA II model has been also extended for PC beams with FRP prestressing tendons, with and without FRP shear reinforcement [45]. The modifications described above for RC beams with FRP bars are applicable for this case, except that $V_{c,min}$ (Eq. 15b) is applicable in the case of PC beams with FRP prestressing tendons, as the prestressing action enhances the shear transfer across the critical crack. An additional particularity of beams with FRP tendons is that, as evidenced by experimental tests [79], they can potentially fail due to excessive slip of the tendon at the critical crack (shear-bond failure), owing to bond characteristics that are in many cases inferior to those of steel tendons. This type of failure will occur if the available bond length between the critical shear crack and the free end of the beam (l_{av}) is lower than the length required to develop the tensile force of the FRP tendon at the critical crack (l_{req}). Bond failure initiation will reduce the prestressing force and, as a result, the shear strength. This will also displace the position of the critical shear crack closer to the support. When $l_{av} < l_{req}$, an iterative procedure is needed to calculate the reduced value of the prestressing force P that will satisfy $l_{av}=l_{req}$ at the shear-bond failure. The available length l_{av} is the sum of the beam offset measured from the center of the support (e) and the position of the critical crack ($s_{cr} = M_{cr}/V_R$), while l_{req} is obtained by enforcing equilibrium along the bonded length and at the critical shear crack section [45]:

$$l_{req} = \frac{F_p}{u\ \tau_{max}} \tag{40}$$

$$F_p = \frac{M_{cr} + 0.85V_{cu}\ d + 0.2125V_{fu}\ d}{z} \tag{41}$$

where u is the nominal perimeter of the tendon, τ_{max} is the bond strength of the tendon, and F_p is the tensile force of the tendon at the critical crack.

A database of 55 tests has been used to assess the accuracy of the model extension for PC beams with FRP prestressing tendons. Most of the tests are on slender beams, but some non-slender elements (a/d<2.5) are also included in the database. Among the non-slender beams, there are beams without shear reinforcement which fail in shear in the absence of flexural cracking, due to the prestressing action. The correction factor for non-slender beams K_{ad} described in Eq. (35) was derived for the CCCM, and it is specific for beams cracked in flexure. An analogous correction factor $K_{ad,u}$ accounting for non-slender effects is proposed to modify the shear strength of uncracked beams V_{Rd} obtained with Eq. (29). The term $K_{ad,u}$ was derived in [45] based on an idealization of the arch and beam actions in non-slender uncracked beams:

$$K_{ad,u} = 1 + 2(1 - 0.4\ \frac{a}{d}) \geq 1 \tag{42}$$

The results of the model estimations for PC beams with FRP reinforcement are summarized in Table 6. As shown, the scatter of the results for PC beams is slightly higher than that for RC beams, consistent with trends observed for steel reinforcement. Notably, the model extension accounting for potential tendon slip is capable of predicting three out of the five shear-bond failures reported in the tests by [79], with the mean experimental-to-predicted strength ratio of 1.05 for these five tests and only one unsafe prediction (ratio < 1).

8.3. Steel Fiber Reinforced Concrete (SFRC) slender and non-slender beams without stirrups

The extension of the proposed model to slender and non-slender SFRC beams [40] was developed in collaboration with researchers from the University of Messina (Italy). The incorporation of steel fibers into concrete mixtures enhances shear behavior by delaying crack formation and improving the post-cracking tensile response. These enhanced mechanical properties significantly increase the shear strength of RC beams, as supported by numerous experimental studies [80–82].

The contribution of steel fibers was integrated into the equilibrium equations of the Multi-Action Shear Model (MASM). The residual tensile stresses of fiber reinforced concrete were addressed through a simplified formulation, which allowed the model to account for an improved compression chord contribution, direct shear transfer through the fiber-bridging effect along the critical shear crack, and enhanced dowel action provided by the fibers. Although these effects were initially modeled at the MASM level, the final expressions were compactly reformulated in [40], resulting in a practical LoA II procedure. The main equations for this extension are summarized in Table 8 and Figure 13, offering a

TABLE 8.
Summary of the LoA II for beams with Steel Fiber Reinforced Concrete without stirrups

	Main expressions	
Concrete contribution	$V_{cu} = [\zeta \frac{x}{d} k_{ad}(0.84–0.10 \frac{\sigma_{tu}}{f_{ct}})+0.08+1.10 \frac{\sigma_{tu}}{f_{ct}}] \frac{f_{ct}}{\gamma_v} b_{v,eff} d$	(43)
Maximum shear strength (strut crushing)	$V_{Rd,max} = \alpha_{cw} b_w z \nu_1 f_{cd} \frac{cot\theta}{1+cot^2\theta} \approx 0.225 f_{cd} b_w d$	(44)
Factors	***Expressions***	
Relative neutral axis depth	$\frac{x}{d} = \frac{x_0}{d} = \alpha_e \rho_{l,b} \left(-1+\sqrt{1+\frac{2}{\alpha_e \rho_{l,b}}}\right) \approx 0.75 (\alpha_e \rho_{l,b})^{1/3}$	(45)
Relative neutral axis depth	$\frac{\sigma_{tu}}{f_{ct}} = 2\eta_0 \eta_1 F_\tau \leq 1$	(46)

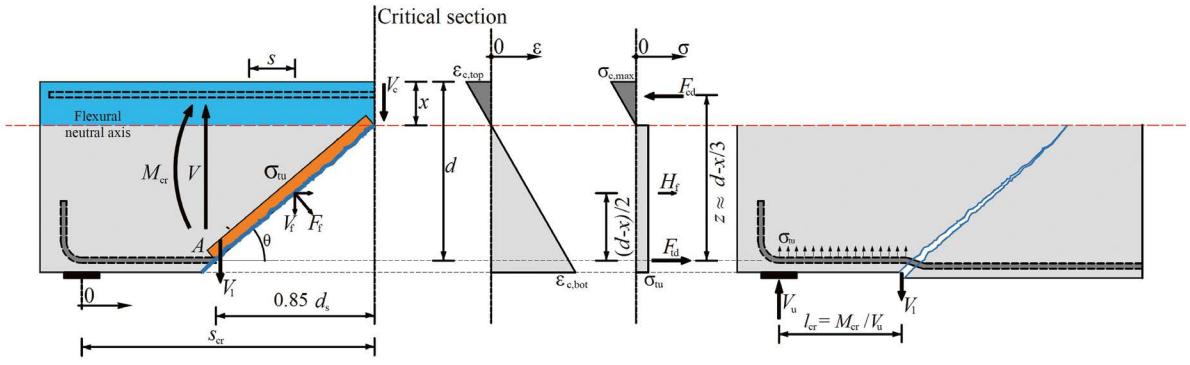

Figure 13. Graphical summary of the extension for SFRC beams without stirrups.

straightforward approach for designers while maintaining accuracy in predicting the shear strength of SFRC beams, both for slender and non-slender beams.

For non-slender SFRC beams, the Kad factor in Eq. (43), given by Eq. (35), adjusts the shear strength to account for arching action. Additionally, the concrete contribution is expressed as proportional to the relative neutral axis depth of an equivalent beam made with conventional concrete (Eq. (42)).

The non-dimensional average residual tensile stress of fibrous concrete in tension, σ_{tu}, is derived from the constitutive law proposed by Lim et al. [83] and is summarized in Eq. (46). Detailed definitions of the involved parameters are provided in the Notations section, while further derivations and explanations can be found in [40].

To validate this model, a database compiled by Lantsoght [80,84] was utilized. The structural parameters in the database vary over a wide range; however, the mechanical characterization of SFRC was not reported. Nevertheless, when experimental results for the post-cracking tensile stress of SFRC are available, they are often obtained using different experimental protocols, making homogenization of the data challenging [80]. Practical values of the fiber volume fraction (V_f) are used (0.5–1.5%), which result in workable mixes and serve the purpose of partially replacing conventional steel reinforcement.

Table 9 summarizes the correlation between experimental and predicted shear strengths for the entire database and specific subsets. The correlations are satisfactory, and they can be compared with those of different code procedures detailed in [40].

TABLE 9.
Comparison of tests results vs. Lantsoght database [80,84].

Database or subset	*#*	*LoA II*	
		Mean	*CoV*
All beams	488	1.17	23.8%
Only beams failing in shear according to the model (flexural check)	324	1.18	24.7%
Failing in shear with $a/d \geq 2.5$	223	1.15	25.6%
Failing in shear with $a/d < 2.5$	101	1.24	22.5%

8.4. RC beams without stirrups subjected to fatigue loads

Shear fatigue failures in reinforced concrete elements without shear reinforcement can govern the design of structures subjected to a high number of load cycles, such as wind towers, offshore structures, bridge decks, precast slabs for railways tracks, and similar applications.

The study of shear fatigue behavior in RC elements without shear reinforcement has a long history, and the associated failure modes are well understood. In 1958, Chang and Kesler [85,86] classified these failure modes into two main groups: the first involves fatigue failure of the longitudinal reinforcement under tension, while the second occurs when the compression zone at the top of the diagonal (shear) crack becomes too small to resist the applied load, due to combined compression and shear stresses.

The MASM/CCCM models define failure using Kupfer's envelope, which considers a combination of compressive and tensile stresses, although tensile stresses primarily govern. As such, the concrete contribution to shear resistance is consist-

ently expressed as a function of the concrete tensile strength in all proposed models (see Eqs. (2), (15), (23), (31), and (43)). This was the foundational assumption for extending the CCCM model (LoA II) to RC beams without stirrups subjected to fatigue loads [41].

Different approaches were employed to account for the reduction of the shear strength under fatigue loading. In the first one, the Model Code 2010 [87] expression for the degradation of concrete tensile strength due to the number of load cycles, N, was used. This relationship is expressed as shown in Eq. (47):

$$\sigma_{ct,max} = f_{ct}\left(1 - \frac{log\ N}{12}\right) \tag{47}$$

An alternative approach, based on Fernández-Ruiz et al. [88], applied Fracture Mechanics principles for quasi-brittle materials. This model considers the ratio of maximum to reference shear strength, V_{max}/V_{ref}, as a function of the load cycle ratio, $R = V_{min}/V_{max}$, and the number of load cycles, N, as expressed in Eq. (48):

$$\frac{V_{max}}{V_{ref}} = \eta \frac{1}{R + N^{\frac{1}{m}}(1-R)} \leq 0.5 \tag{48}$$

In this equation, m is an empirically derived coefficient equal to 17, and the threshold of 0.5 also refer to the average test response. The authors [88] recognized that these values could be adapted, if necessary, to respect a target safety level. The term η is a multiplying factor of static strength due to the loading rate, considered equal to 1 in [41] and in this paper, balancing two considerations: the implicit value of 0.9 suggested by Eurocode 2 [68] to reflect long-term effects on compressive strength, and the value of 1.1 proposed by Fernández-Ruiz et al. [88] to account for the increased concrete compressive strength observed in tests conducted at a loading rate of 1 Hz compared to failure times of approximately 1 hour in standard beam tests. Further details on this topic can be found in [41].

For facilitating the comparison with tests results, Eq. (48) can be reformulated in terms of V_{min}/V_{ref} (see Eq. 49):

$$\frac{V_{max}}{V_{ref}} = \eta N^{-1/m} + \frac{V_{min}}{V_{ref}}\left(1 - N^{-1/m}\right) \leq 0.5 \tag{49}$$

A database of fatigue tests on shear-critical beams, comprising 87 tests, was used to validate both approaches. This database, originally developed in [89], was later expanded and published in [88]. The primary results are summarized in Table 10.

The second method, which accounts for the load cycle ratio, R, provides slightly better and more consistent results across the entire range of log N values analysed (see Figure 14). Nevertheless, the differences between the two methods are minimal. Further empirical comparisons, presented in terms of Goodman diagrams, are available in [41].

TABLE 10.
Comparison of tests results vs. fatigue tests results.

Method	#	*LoA II*	
		Mean	*CoV*
LoA II with Eq (47)	87	1.15	14.6%
LoA II with Eqs. (48-49)	87	1.19	13.3%

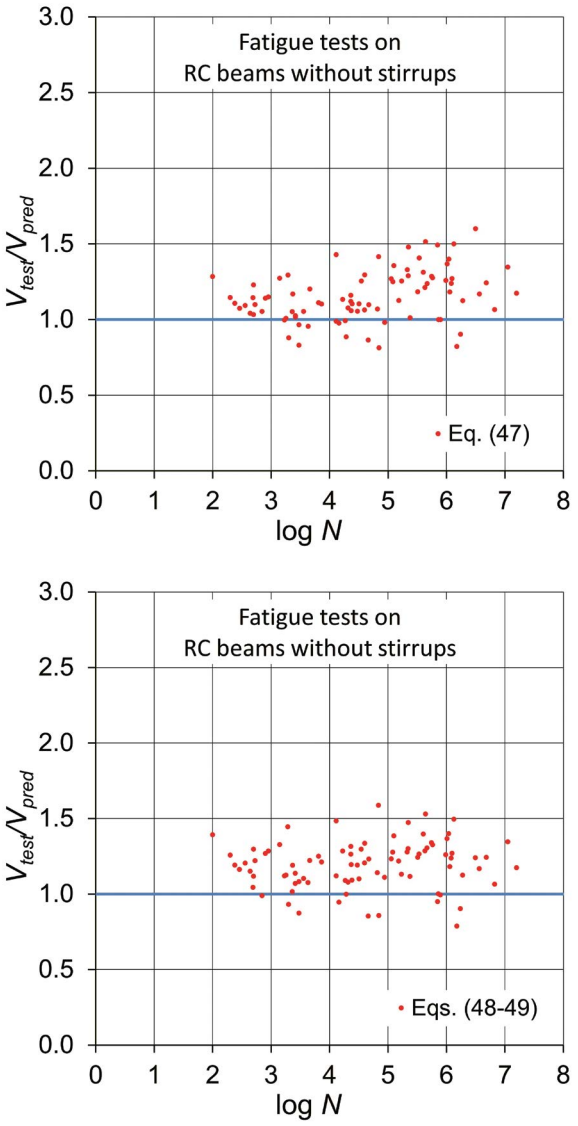

Figure 14. Correlation between predictions and experimental results for the two approaches considered for fatigue loads.

9. CONCLUSIONS

A unified mechanical model for the shear strength of slender and non-slender reinforced and prestressed concrete beams has been developed, applicable to beams with rectangular, T-, or I-shaped sections. Some distinct features of the presented model are:

- The model, based on the Multi-Action Shear Model (MASM), effectively integrates shear transfer actions such as compression chord contribution, residual tensile stresses across the critical crack, dowel action, and transversal reinforcement effects (if present).
- The Levels-of-Approximation (LoA) framework enables the application of the model in a wide range of structural design and assessment scenarios, with increasing complexity from LoA 0 (preliminary design) to LoA III (detailed assessment). Specifically, LoA III is based on the MASM,

and LoA II on the Compression Chord Capacity Model (CCCM). All LoAs provide continuous models for members with or without shear reinforcement.

- As highlighted in the introductory section of this paper, different mechanical approaches are valid for addressing the shear failure problem, and various models should be viewed as complementary rather than contradictory. For instance, for members with moderate or high amounts of shear reinforcement, variable-angle truss models based on plasticity offer a quick and practical design approach, particularly when torsion is present.
- The extension of LoA II (CCCM) to cover specific cases, such as the shear strength of non-slender beams, RC and PC beams reinforced with fiber reinforced polymers (FRP) bars, steel fiber reinforced concrete (SFRC) members, and fatigue loads for RC beams without stirrups, has been also presented.
- Validation of the model using 2,714 experimental tests from 14 databases has shown its accuracy and versatility, with improved prediction consistency and reduced scatter at higher LoAs.

This work contributes a robust tool for the design and assessment of structural concrete elements, offering a systematic approach that combines advanced mechanics with engineering practice. Looking ahead, future work will focus on conducting a comprehensive reliability analysis to assess the sensitivity and robustness of the model under varying conditions, particularly considering uncertainties in material properties, geometry, and loading. Such an analysis would be important for calibrating the models to the levels recommended by current standards and determining the most appropriate safety format, whether through partial safety factors or a global factor. Further research could also explore the application of the model to more complex geometries or hybrid materials, such as combinations of steel, FRP, and SFRC. Additionally, integrating the model into advanced structural design software could greatly enhance its usability in practical engineering scenarios.

Acknowledgements

This paper is dedicated to Prof. Antonio Marí, the leading force behind our 12 years of research on shear strength and the scientific father of the Multi-Action Shear Model. His guidance, wisdom, and vision have been an inspiration to all of us, and we owe him the deepest gratitude as our master, mentor and friend throughout these years. Additionally, we extend this dedication to Prof. Hugo Corres, whose insightful discussions and valuable contributions to the topic of shear strength have greatly enriched our work.

We would also like to acknowledge the financial support provided by grants TED2021-130272B-C21 / TED2021-130272B-C22 funded by MICIU/AEI/10.13039/501100011033 and the European Union Next Generation/PRTR, as well as grants PID2021-123701OB-C21 / PID2021-123701OB-C22 funded also by MICIU/AEI/10.13039/501100011033 and by ERDF/EU.

Notations

a	shear span, equal to $M_{Ed,max}/V_{Ed,max}$, where $M_{Ed,max}$ and $V_{Ed,max}$ are the maximum absolute values of the internal forces in the region between the maximum bending moment and the zero bending moment in which the considered section is located. This is equivalent to the distance from the support to the resultant of the loads producing shear at that support. Design values for uniformly distributed load, $a=0.25L$ (simple supported); $a=0.5L$ (cantilever); $a=0.2L$ (sagging moment regions in continuous beams); $a=0.15L$ (hogging moment regions in continuous members)
b	cross-section width. For T/I-sections, flexural effective compression flange width
b_{tens}	tensile flange width
$b_{v,eff}$	effective width for shear strength calculation
b_w	web width for T/I/L beams; for rectangular beams $b_w = b$
d	effective depth, $d=\frac{A_s d_s + A_p d_p}{A_s + A_p}$
d_0	minimum effective depth for size effect factor, d_0 = d≥100 mm
d_f	fiber diameter
d_{max}	maximum aggregate size
d_s	distance from maximum compressed concrete fiber to the centroid of mild steel tensile reinforcement. For elements with only prestressed reinforcement, $d_s = d_p$
d_p	distance from maximum compressed concrete fiber to the centroid of prestressing tendons placed at the tension zone
f_{cd}	design compressive strength of concrete
f_{ck}	characteristic compressive strength of concrete ($f_{ck} \leq 100$ MPa)
f_{cm}	mean compressive strength of concrete
f_{ct}	tensile strength of concrete, as per second generation of Eurocode 2 in this paper: $f_{ct}=f_{ctm}= 0.3f_{ck}^{2/3}$ if $f_{ck} \leq 50$ MPa, and $f_{ct}=f_{ctm}=1.1f_{ck}^{1/3}$ if $f_{ck} > 50$ MPa
f_{tu}	ultimate strength of FRP transverse reinforcement
f_{ywd}	design yield strength of shear reinforcement
h	overall cross-section depth
h_f	compression flange height. For haunched T/I/L beams, flange height + half the haunch
$h_{f,tens}$	tensile flange height. In T, I or L beams with haunches, $h_{f,tens}$ can be considered the flange height plus half the haunch
l_{av}	available bond length of prestressing tendon between critical shear crack and free end of the beam
l_c	critical fiber length, $\frac{\sigma_{fy} d_f}{2\tau_f}$
l_{req}	bond length required to develop the tensile force of prestressing tendon at the critical crack
s	stirrups spacing
u	nominal perimeter of FRP tendon.
x	neutral axis depth assuming zero concrete tensile strength
x_0	neutral axis depth for RC or PC members assuming $P = 0$
y_t	distance from the concrete section centroid to the most tensioned fiber
z	inner lever arm, approximate value $z \approx 0.9d$ may normally be used

A_c concrete cross-sectional area

A_p prestressing steel (tensile zone) cross-sectional area

A_s mild steel reinforcement (tensile zone) cross-sectional area

A_{sw} shear reinforcement cross-sectional area

E_{cm} secant modulus of elasticity of concrete, $E_{cm}=kE\ fcm^{1/3}$; for concrete with quartzite aggregates k_E = 9500 (value assumed in this paper)

E_s elastic modulus of mild reinforcement (200 GPa)

E_p elastic modulus of prestressing steel (195 GPa, if unspecified)

F_p tensile force of FRP tendon at critical crack.

F_τ fiber factor, $F_\tau=\beta_\tau\ V_f \frac{l_f}{d_f}$

G_f concrete fracture energy, $G_f = 0.028 f_{cm}^{0.18}\ d_{max}^{0.32}$

I_c second moment of area

K_{ad} factor that accounts for ratio between shear strengths of cracked non-slender and slender beams

$K_{ad,u}$ factor that accounts for ratio between shear strengths of uncracked non-slender and slender beams

K_p strength factor for axial load (including prestressing) and bending moment interaction

K_T strength factor for T/I-sections relative to rectangular beams

L_f fiber length

M_{Ed} design bending moment (positive)

N_{Ed} design axial/prestressing force (compression positive)

P prestressing tendon force after losses

S_c first moment of area above the centroid

V_{cu} concrete contribution to the shear strength

V_f volumetric percentage of fibers

V_{fu} shear FRP reinforcement contribution to the shear strength

V_{su} shear reinforcement contribution to the shear strength

V_{Ed} design shear force in the section

V_{Rd} design shear resistance of the member

$V_{Rd,max}$ maximum design shear resistance limited by strut crushing

α angle between shear reinforcement and beam axis perpendicular to the shear force

α_{cw} coefficient for stress in the struts: α_{cw}=1 for non-prestressed structures; $\alpha_{cw}=1+\sigma_{cp}/f_{cdfor}$ $0\le\sigma_{cp}\le0.25f_{cd}$; α_{cw}=1.25 for $0.25f_{cd}<\sigma_{cp}\le0.50f_{cd}$; and $\alpha_{cw}=2.5(1-\sigma_{cp}/f_{cd})$ for $0.50f_{cd}<\sigma_{cp}\le f_{cd}$

α_e modular ratio, $\alpha_e=E_s/E_{cm}$

α_l prestressing force transfer degree, which is ≤ 1.0 for pretensioned tendons, and equal to 1.0 for other types of prestressing

β_τ ratio of mean fiber-matrix shear stress to tensile strength, $\beta\tau=\tau_f/f_{ct}$. In the typical case of concrete matrix, β_τ adopts the value of 1.45 for hooked fibers and 0.70 for straight fibers. Mean value considered for crimped fibers

δ_p angle between prestressed tendon axis and beam axis

γ_v partial factor for concrete shear contribution. According to the 2nd generation of EC2, = 1.4 for persistent and transient design situation or fatigue. For accidental design situation 1.15. Necessary to carry out a reliability analysis to confirm these values.

η_0 fiber orientation factor, η_0 = 0.405.

η_1 fiber length efficiency factor. If $L_f \le l_c \rightarrow \eta_1 = 0.5$; otherwise $\eta_1=1-\frac{L_c}{2L_f}$

υ_1 strength reduction factor for concrete cracked in shear, υ_1 = 0.6 for $f_{ck} \le 60$ MPa and $\upsilon_1 = 0.9\text{-}f_{ck}/200$ for $f_{ck} > 60$ MPa

θ strut angle with respect beam axis

$\rho_{l,b}$ longitudinal tensile reinforcement ratio relative to effective depth d and the width b. For members with mild steel reinforcement and tendons, $\alpha_e\ \rho_{l,b}=\alpha_{e,s}\ \rho_{s,b}+\alpha_{e,p}\ \rho_{p,b}$ being $\alpha_{e,s}=E_s/E_{cm}$, $\alpha_{e,p}=E_p/E_{cm}$, $\rho_{s,b}=A_s/b_d$, $\rho_{p,b}=A_p/\ b_d$ and b the width of the cross-section. For the case of unbonded tendons, A_p = 0.

$\rho_{l,w}$ same as $\rho_{l,w}$ but relative to web width b_w

σ_{cp} concrete compressive stress at the centroid due to axial/prestressing load,$\sigma_{cp} = N_{Ed}/A_c$ (N_{Ed}>0 compression)

σ_{sy} steel fiber yield strength

σ_t mean value of the tensile stresses in the FRP stirrups crossing the shear critical crack

τ_f mean fiber-matrix shear stress. See definition of β_τ

τ_{max} bond strength of FRP tendon.

ζ combined size and slenderness effect factor (LoAs II and III)

ζ' size effect factor for LoA I, equal to ζ but assuming a/d = 4

References

[1] Mörsch E. Concrete-Steel Construction (Der Eisenbetonbau), authorized translation form the third German Edition. New York: The Engineering News Publishing Company; 1909.

[2] Faber O. Researches on Reinforced Concrete Beams with New Formulae for Resistance to Shear. Parts I, II, III and shear tests (1914 series). Concrete and Constructional Engineering (London) 1916;11:233–605.

[3] Fenwick RC. The shear strength of reinforced concrete beams. University of Canterbury, 1966.

[4] Fenwick RC, Paulay T. Mechanisms of shear resistance of concrete beams. ASCE J Struct Div 1968;94:2325–50.

[5] ACI-ASCE Committee 426. The Shear Strength of Reinforced Concrete Members. ACI Journal Proceedings, vol. 70, ACI; 1973, p. 1091–187.

[6] Walraven JC. Fundamental analysis of aggregate interlock. ASCE J Struct Div 1981;107:2245–70.

[7] Haskett M, Oehlers DJ, Mohamed Ali MS, Sharma SK. Evaluating the shear-friction resistance across sliding planes in concrete. Eng Struct 2011;33:1357–64. https://doi.org/10.1016/j.engstruct.2011.01.013.

[8] Walraven JC. Aggregate interlock: A theoretical and experimental analysis. Delft University, 1980.

[9] Leonhardt F. Shear and torsion in prestressed concrete. VI FIP Congresss Prague, vol. Session IV, 1970.

[10] Regan PE. Research on shear: a benefit to humanity or a waste of time? Structural Engineer 1993;71:337.

[11] Belarbi A, Kuchma DA, Sanders DH. Proposals for New One-Way Shear Equations for the 318 Building Code. Concrete International 2017;39:29–32.

[12] Li Y-A, Hsu TTC, Hwang S-J. Shear Strength of Prestressed and Nonprestressed Concrete Beams. Concrete International 2017;39:53–7.

[13] Park H-G, Choi K-K. Unified Shear Design Method of Concrete Beams Based on Compression Zone Failure Mechanism. Concrete International 2017;39:59–63.

[14] Reineck K-H. Proposal for ACI 318 Shear Design Members without Shear Reinforcement. Concrete International 2017;39:65–70.

[15] Bentz EC, Collins MP. Updating the ACI Shear Design Provisions. Concrete International 2017;39:33–8.

[16] Cladera A, Marí A, Bairán J-M, Oller E, Ribas C. One-Way Shear Design Method Based on a Multi-Action Model A compromise between simplicity and accuracy. Concrete International 2017;39:40–6.

[17] Frosch RJ, Yu Q, Cusatis G, Bažant ZP. A Unified Approach to Shear Design. Concrete International 2017;39:47–52.

[18] Campana S, Ruiz MF, Anastasi A, Muttoni A. Analysis of shear-transfer actions on one-way RC members based on measured cracking pattern and failure kinematics. Magazine of Concrete Research 2013;65:386–404. https://doi.org/10.1680/macr.12.00142.

[19] Cavagnis F, Fernández Ruiz M, Muttoni A. Shear failures in reinforced concrete members without transverse reinforcement: An analysis of the critical shear crack development on the basis of test results. Eng Struct 2015;103:157–73. https://doi.org/10.1016/J.ENGSTRUCT.2015.09.015.

[20] Cavagnis F, Fernández Ruiz M, Muttoni A. An analysis of the shear-transfer actions in reinforced concrete members without transverse reinforcement based on refined experimental measurements. Structural Concrete 2018;19:49–64. https://doi.org/10.1002/SUCO.201700145.

[21] Huber P, Huber T, Kollegger J. Investigation of the shear behavior of RC beams on the basis of measured crack kinematics. Eng Struct 2016;113:41–58. https://doi.org/10.1016/J.ENGSTRUCT.2016.01.025.

[22] Huber T, Huber P, Kollegger J. Influence of aggregate interlock on the shear resistance of reinforced concrete beams without stirrups. Eng Struct 2019;186:26–42. https://doi.org/10.1016/J.ENGSTRUCT.2019.01.074.

[23] Kani MW, Huggins MW, Wittkopp RR. Kani on shear in reinforced concrete. Dept. of Civil Engineering, University of Toronto; 1979.

[24] Montoya-Coronado LA, Ribas C, Ruiz-Pinilla JG, Cladera A. Time-history analysis of aggregate interlock in reinforced concrete beams without stirrups. Eng Struct 2023;283:115912. https://doi.org/10.1016/j.engstruct.2023.115912.

[25] Zararis PD, Papadakis GC. Diagonal shear failure and size effect in RC beams without web reinforcement. Journal of Structural Engineering 2001;127:733–42. https://doi.org/10.1061/(ASCE)0733-9445(2001)127:7(733).

[26] Tureyen AK, Frosch RJ. Concrete Shear Strength: Another Perspective. ACI Struct J 2003;100:609–15.

[27] Park HG, Kang S, Choi KK. Analytical model for shear strength of ordinary and prestressed concrete beams. Eng Struct 2013;46:94–103. https://doi.org/10.1016/j.engstruct.2012.07.015.

[28] Muttoni A, Fernandez-Ruiz M. Shear Strength of Members without Transverse Reinforcement as Function of Critical Shear Crack Width. ACI Struct J 2008;105:163–72.

[29] Collins MP, Bentz EC, Sherwood EG, Xie L. An adequate theory for the shear strength of reinforced concrete structures. Magazine of Concrete Research 2008;60:635–50.

[30] Bairán JM, Marí A, Cladera A. Analysis of shear resisting actions by means of optimization of strut and tie models taking into account crack patterns. Hormigón y Acero 2018;69:197–206. https://doi.org/10.1016/j.hya.2017.04.009.

[31] Ribas C, Cladera A. Experimental study on shear strength of beam-and-block floors. Eng Struct 2013;57:428–42. https://doi.org/10.1016/j.engstruct.2013.10.001.

[32] Marí A, Cladera A, Oller E, Bairán J. Shear design of FRP reinforced concrete beams without transverse reinforcement. Compos B Eng 2014;57:228–41. https://doi.org/10.1016/j.compositesb.2013.10.005.

[33] Oller E, Marí A, Bairán JM, Cladera A. Shear design of reinforced concrete beams with FRP longitudinal and transverse reinforcement. Compos B Eng 2015;74:104–22. https://doi.org/10.1016/j.compositesb.2014.12.031.

[34] Marí A, Bairán J, Cladera A, Oller E, Ribas C. Shear-flexural strength mechanical model for the design and assessment of reinforced concrete beams. Structure and Infrastructure Engineering 2015;11:1399–419. https://doi.org/10.1080/15732479.2014.964735.

[35] Cladera A, Marí A, Ribas C, Bairán J, Oller E. Predicting the shear–flexural strength of slender reinforced concrete T and I shaped beams. Eng Struct 2015;101:386–98. https://doi.org/10.1016/j.engstruct.2015.07.025.

[36] Marí A, Bairán JM, Cladera A, Oller E. Shear Design and Assessment of Reinforced and Prestressed Concrete Beams Based on a Mechanical Model. Journal of Structural Engineering 2016;142:04016064. https://doi.org/10.1061/(ASCE)ST.1943-541X.0001539.

[37] Marí A, Cladera A, Bairán J, Oller E, Ribas C. Un modelo unificado de resistencia a flexión y cortante de vigas esbeltas de hormigón armado bajo cargas puntuales y repartidas. Hormigón y Acero 2014;65:247–65. https://doi.org/10.1016/j.hya.2014.11.001.

[38] Cladera A, Marí AR, Bairán JM, Ribas C, Oller E, Duarte N. The compression chord capacity model for the shear design and assessment of reinforced and prestressed concrete beams. Structural Concrete 2016;17:1017–32. https://doi.org/10.1002/suco.201500214.

[39] Bairán JM, Menduiña R, Marí A, Cladera A. Shear strength of non-slender reinforced concrete beams. ACI Struct J 2020;117:277–89. https://doi.org/10.14359/51721369.

[40] Marí A, Spinella N, Recupero A, Cladera A. Mechanical model for the shear strength of steel fiber reinforced concrete (SFRC) beams without stirrups. Mater Struct 2020;53:28. https://doi.org/10.1617/s11527-020-01461-4.

[41] Cladera A, Ribas C, Oller E, Marí A. Shear fatigue strength of reinforced concrete members without transverse reinforcement according to the compression chord capacity model. Eng Struct 2020;211:110495. https://doi.org/10.1016/j.engstruct.2020.110495.

[42] Cladera A, Marí A, Ribas C. Mechanical model for the shear strength prediction of corrosion-damaged reinforced concrete slender and non slender beams. Eng Struct 2021;247:113163. https://doi.org/10.1016/j.engstruct.2021.113163.

[43] Frontera A, Cladera A. Predicción a largo plazo de la resistencia a cortante de vigas de hormigón armado basada en un modelo mecánico considerando la corrosión de la armadura. Hormigón y Acero 2024;75:79–90. https://doi.org/10.33586/hya.2024.3136.

[44] Frontera A, Cladera A. Long-term shear strength of RC beams based on a mechanical model that considers reinforcing steel corrosion. Structural Concrete 2023;24:25–40. https://doi.org/10.1002/suco.202200428.

[45] Oller E, Murcia-Delso J, Marí A, Legasa T. Theoretical Model for the Shear Strength of Prestressed Concrete Beams with FRP Tendons. Journal of Composites for Construction 2024;28. https://doi.org/10.1061/JCCOF2.CCENG-4390.

[46] Marí A, Cladera A, Oller E, Bairán JM. A punching shear mechanical model for reinforced concrete flat slabs with and without shear reinforcement. Eng Struct 2018;166:413–26. https://doi.org/10.1016/j.engstruct.2018.03.079.

[47] Marí AR, Fernández PG, Oller E, Cladera A. Punching-Shear Strength of Reinforced Concrete Slabs Subjected to Concentric Transverse Loads and In-Plane Tensile Forces. SP-357: Punching Shear of Concrete Slabs: Insights from New Materials, Tests, and Analysis Methods, American Concrete Institute; 2023, p. 139–59. https://doi.org/10.14359/51738764.

[48] Rius JM, Cladera A, Mas B, Ribas C. Shear behaviour of beams strengthened using different Ni-Ti-Nb shape memory alloy wire configurations and design proposal based on the compression chord Capacity model (CCCM). Eng Struct 2022;268:114724. https://doi.org/10.1016/j.engstruct.2022.114724.

[49] Cladera A, Montoya-Coronado LA, Ruiz-Pinilla JG, Ribas C. Shear strengthening of slender reinforced concrete T-shaped beams using iron-based shape memory alloy strips. Eng Struct 2020;221:111018. https://doi.org/10.1016/j.engstruct.2020.111018.

[50] Ribas González CR, D'Antino T, Sneed LH. Shear Strength Model for Reinforced Concrete Beams with U-Wrapped FRCM Composites Based on the Critical Shear Crack Width Evolution. Journal of Composites for Construction 2025;29:04025021. https://doi.org/10.1061/JCCOF2.CCENG-5040.

[51] Marí A. Questions on Shear Behavior of Structural Concrete and Answers Provided by Mechanical Models. The Challenge of Performance-Based Shear Design. Hormigón y Acero 2023;75:7–24. https://doi.org/10.33586/hya.2023.3116.

[52] Sigrist V, Bentz E, Ruiz MF, Foster S, Muttoni A. Background to the fib Model Code 2010 shear provisions – part I: beams and slabs. Structural Concrete 2013;14:195–203. https://doi.org/10.1002/suco.201200066.

[53] Muttoni A, Fernández-Ruiz M. Levels-of-Approximation Approach in Codes of Practice. Structural Engineering International 2012;22:190–4. https://doi.org/10.2749/101686612X13291382990688.

[54] Carmona JR, Ruiz G, del Viso JR. Mixed-mode crack propagation through reinforced concrete. Eng Fract Mech 2007;74:2788–809. https://doi.org/10.1016/j.engfracmech.2007.01.004.

[55] Yu Q, Le J-L, Hubler MH, Wendner R, Cusatis G, Bažant ZP. Comparison of main models for size effect on shear strength of reinforced and prestressed concrete beams. Structural Concrete 2016;17:778–89. https://doi.org/10.1002/suco.201500126.

[56] Kupfer HB, Gerstle KH. Behavior of concrete under biaxial stresses. Journal of the Engineering Mechanics Division 1973;99:853–66.

[57] Bažant ZP, Yu Q, Gerstle W, Hanson J, Ju JW. Justification of ACI 446 Proposal for Updating ACI Code Provisions for Shear Design of Reinforced Concrete Beams. Structural Journal 2007;104:601–10.

[58] Pérez JL, Cladera A, Rabuñal JR, Martínez-Abella F. Optimization of existing equations using a new Genetic Programming algorithm: Application to the shear strength of reinforced concrete beams. Advances in Engineering Software 2012;50:82–96. https://doi.org/10.1016/j.advengsoft.2012.02.008.

[59] Cladera A, Perez-Ordonez JL, Martinez-Abella F. Shear strength of RC beams. Precision, accuracy, safety and simplicity using genetic programming. Computers and Concrete 2014;14:479–501. https://doi.org/10.12989/cac.2014.14.4.479.

[60] Marí Bernat AR, Cladera Bohigas A, Bairán García JM. Effects of axial forces and prestressing on the shear strength of structural concrete members. Congreso de la de la Asociación Científico-Técnica del Hormigón Estructural (ACHE) 2017, 2017, p. 1–10.

[61] Evans RH, Schumacher EG. Shear Strength of Prestressed Beams Without Web Reinforcement. ACI Journal Proceedings 1963;60:1621–42. https://doi.org/10.14359/7907.

[62] Elzanaty AH, Nilson AH, Slate FO. Shear Capacity of Prestressed Concrete Beams Using High-Strength Concrete. ACI Journal 1986;83:359–68. https://doi.org/10.14359/10436.

[63] Choulli Y, Marí AR, Cladera A. Shear behaviour of full-scale prestressed i-beams made with self compacting concrete. Materials and Structures/Materiaux et Constructions 2008;41. https://doi.org/10.1617/s11527-007-9225-1.

[64] Reineck K-H, Bentz EC, Fitik B, Kuchma DA, Bayrak O. ACI-DAfStb database of shear tests on slender reinforced concrete beams without stirrups. ACI Struct J 2013;110:867–75.

[65] Reineck K-H, Bentz E, Fitik B, Kuchma DA, Bayrak O. ACI-DAfStb Databases for Shear Tests on Slender Reinforced Concrete Beams with Stirrups. ACI Struct J 2014;111:1147–56.

[66] ACI-DAfStb 617. ACI-DAfStb databases 2015 on shear tests for evaluating relationships for the shear design of structural concrete members without and with stirrups. Berlin: Beuth Verl; 2015.

[67] British Standards Institution BSI. BSI Standards Publication Eurocode 2 - Design of concrete structures. BSI Standards Publication 2023:408.

[68] Eurocode 2. EC2 Design of concrete structures. Part 1: General rules and rules for buildings. European Committee for Standardization (CEN); 2002.

[69] Fernández-Montes D, González Valle E, Díaz Heredia E. Influence of axial tension on the shear strength of floor joists without transverse reinforcement. Structural Concrete 2015;16:207–20. https://doi.org/10.1002/suco.201400063.

[70] Jørgensen HB, Hoang LC, Fabrin LS, Malgaard J. Influence of High Axial Tension on the Shear Strength of non-shear RC Beams. Proceedings of the International IABSE conference: Assessment, Upgrading, Refurbishment of Infrastructures, 2013.

[71] Kani G. The riddle of shear failure and its solution. ACI Journal Proceedings 1964;61:441–67.

[72] Vollum RL, Fang L. Shear enhancement in RC beams with multiple point loads. Eng Struct 2014;80:389–405. https://doi.org/10.1016/j.engstruct.2014.09.010.

[73] Reineck KH, Todisco L. Database of shear tests for non-slender reinforced concrete beams without stirrups. ACI Struct J 2014;111:1363–71. https://doi.org/10.14359/51686820.

[74] Todisco L, Reineck K-H, Bayrak O. Database with Shear Tests on Non-Slender Reinforced Concrete Beams with Vertical Stirrups. Structural Journal 2015;112:761–9.

[75] Todisco L, Bayrak O, Reineck KH. ACI-DAfStb database for tests on deep beams and comparisons with code provisions. Structural Concrete 2018;19:296–304. https://doi.org/10.1002/suco.201700061.

[76] Guadagnini M. Shear behavior and design of FRP RC beams. University of Sheffield, 2002.

[77] Japanese Society of Civil Engineers (JSCE). Recommendations for design and construction for concrete structures using continuous fibre reinforcing materials. vol. 23. 1997.

[78] ACI Committee 440. 440.1R-15, Guide for the Design and Construction of Structural Concrete Reinforced with Fiber-Reinforced Polymer (FRP) Bars. Farmington Hills MI: American Concrete Institute; 2015.

[79] Kueres S, Will N, Hegger J. Shear strength of prestressed FRP reinforced concrete beams with shear reinforcement. Eng Struct 2020;206:110088. https://doi.org/10.1016/j.engstruct.2019.110088.

[80] Lantsoght E. Database of Shear Experiments on Steel Fiber Reinforced Concrete Beams without Stirrups. Materials 2019;12:917. https://doi.org/10.3390/ma12060917.

[81] Minelli F, Conforti A, Cuenca E, Plizzari G. Are steel fibres able to mitigate or eliminate size effect in shear? Mater Struct 2014;47:459–73. https://doi.org/10.1617/s11527-013-0072-y.

[82] Dinh HH, Parra-Montesinos GJ, Wight JK. Shear Strength Model for Steel Fiber Reinforced Concrete Beams without Stirrup Reinforcement. Journal of Structural Engineering 2010;137:1039–51. https://doi.org/10.1061/(ASCE)ST.1943-541X.0000362.

[83] Lim TY, Paramasivam P, Lee SL. Bending Behavior of Steel-Fiber Concrete Beams. ACI Struct J 1987;84:524–36. https://doi.org/10.14359/2794.

[84] Lantsoght EOL. Database of experiments on SFRC beams without stirrups failing in shear. 2019. https://doi.org/10.5281/zenodo.2578060.

[85] Chang TS, Kesler CE. Fatigue Behavior of Reinforced Concrete Beams. ACI Journal Proceedings 1958;55:245–54. https://doi.org/10.14359/11352.

[86] Chang TS, Kesler CE. Static and Fatigue Strength in Shear of Beams with Tensile Reinforcement. ACI Journal Proceedings 1958;54:1033–57. https://doi.org/10.14359/11493.

[87] Fédération Internationale du Béton. fib Model Code for Concrete Structures 2010. vol. 1. Lausanne: Ernst & Sohn; 2013.

[88] Fernández-Ruiz M, Zanuy C, Natário F, Gallego JM, Albajar L, Muttoni A. Influence of Fatigue Loading in Shear Failures of Reinforced Concrete Members without Transverse Reinforcement. Journal of Advanced Concrete Technology 2015;13:263–74. https://doi.org/10.3151/jact.13.263.

[89] Gallego JM, Zanuy C, Albajar L. Shear fatigue behaviour of reinforced concrete elements without shear reinforcement. Eng Struct 2014;79:45–57. https://doi.org/10.1016/J.ENGSTRUCT.2014.08.005.

APPENDIX A:

Derivation of LoA II (CCCM) from LoA III (MASM)

A1. Detailed derivation of the main CCCM equation:

In LoA III (MASM), the general equation for the shear strength is given as:

$$V_{Rd} = V_{cu} + V_{su} = (v_c + v_w + v_l)\frac{f_{ct}}{\gamma_v} \cdot b \cdot d + V_{su}$$

Substituting the detailed components:

$$V_{Rd} = \zeta \left\{ \left[\left(0.70 + 0.18K_T + \left(0.20 + 0.50\frac{b}{b_w}\right)v_s\right)\frac{x}{d} + 0.02K_T \right] \frac{b_{v,eff}}{b} K_p + v_w + v_l \right\} \frac{f_{ct}}{\gamma_v} bd + V_{su}$$

For simplification, we assume $K_T = 1$, $K_P = 1$, and adopt safe average values of $v_w = 0.035$ and $v_l = 0.025$. Substituting these values:

$$V_{Rd} = \left\{ \zeta \left[\left(0.88 + \left(0.20 + 0.50\frac{b}{b_w}\right)v_s\right)\frac{x}{d} + 0.02 \right] \frac{b_{v,eff}}{b} + 0.035 + 0.025 \right\} \frac{f_{ct}}{\gamma_v} bd + V_{su}$$

To further simplify, the terms $v_w = 0.035$ and the constant 0.02 are incorporated in the x/d multiplier, assuming an average $z/d = 0.35$. Similarly, $v_l = 0.025$ is added to the vs factor, with an average v_s=0.25. For simplifying reasons, when introducing these constant values inside the parenthesis, the terms $b_{v,eff}/b$ and ζ have been considered equal to 1:

$$V_{Rd} = \left\{ \zeta \left[\left(0.88 + \frac{0.02}{0.35} + \frac{0.035}{0.35} + \left(0.20 + \frac{0.025}{0.35 \cdot 0.25} + 0.50\frac{b}{b_w}\right)v_s\right)\frac{x}{d} \right] \frac{b_{v,eff}}{b} \right\} \frac{f_{ct}}{\gamma_v} bd + V_{su} =$$

$$= \left\{ \zeta \left[\left(1.04 + \left(0.49 + 0.50\frac{b}{b_w}\right)v_s\right)\frac{x}{d} \right] \frac{b_{v,eff}}{b} \right\} \frac{f_{ct}}{\gamma_v} bd + V_{su} \approx$$

$$\approx \zeta \frac{x}{d}\frac{b_{v,eff}}{b}\frac{f_{ct}}{\gamma_v} bd + 0.5\zeta \left(1 + \frac{b}{b_w}\right)v_s \frac{x}{d}\frac{b_{v,eff}}{b}\frac{f_{ct}}{\gamma_v} bd + V_{su} =$$

$$\approx \zeta \frac{x}{d}\frac{f_{ct}}{\gamma_v} b_{v,eff} d + 0.5\zeta \left(1 + \frac{b}{b_w}\right)\frac{V_{su}}{\frac{f_{ct}}{\gamma_v} bd}\frac{x}{d}\frac{b_{v,eff}}{b}\frac{f_{ct}}{\gamma_v} bd + V_{su} =$$

$$= \zeta \frac{x}{d}\frac{f_{ct}}{\gamma_v} b_{v,eff} d + V_{su}\left[1 + 0.5\zeta \left(1 + \frac{b}{b_w}\right)\frac{x}{d}\frac{b_{v,eff}}{b}\right] = \zeta \frac{x}{d}\frac{f_{ct}}{\gamma_v} b_{v,eff} d + V_{su}[1 + \Delta_{Vcu}]$$

The term $\Delta_{Vcu} = 0.5\zeta \left(1 + \frac{b}{b_w}\right)\frac{x}{d}\frac{b_{v,eff}}{d}$ considers the increase in the concrete contribution to the shear strength due to the confinement caused by the stirrups to the compression chord concrete. An average value Δ_{Vcu}=0.4 is adopted to simplify the calculation procedure:

$$V_{Rd} = \zeta \frac{x}{d}\frac{f_{ct}}{\gamma_v} b_{v,eff} d + 1.4V_{su}$$

A2. Detailed derivation of the $V_{cu,min}$ expression

For some cases, v_w is an important shear contribution and the value adopted in A1 (v_w =0.035) is too conservative. This may happen for members, especially one-way slabs, with low values of d or low values of x/d (assumed $x/d < 0.2$ in the following). It has been considered that there is no shear reinforcement:

$$V_{cu,min} = (v_c + v_w)\frac{f_{ct}}{\gamma_v} bd =$$

$$= \left\{ \zeta \left[(0.70 + 0.18K_T)\frac{x}{d} + 0.02K_T \right] \frac{b_{v,eff}}{b} K_p + v_w \right\} \frac{f_{ct}}{\gamma_v} bd =$$

Assuming $K_T = 1$, $K_P = 1$, and substituting E_{cm} and G_f for a 25 MPa compressive strength concrete:

$$V_{cu,min} = \left\{\zeta\left[0.88\frac{x}{d} + 0.02\right]\frac{b_{v,eff}}{b} + 167\frac{f_{ct}}{E_{cm}}\frac{b_w}{b}\left(1 + \frac{2 \cdot G_f \cdot E_{cm}}{f_{ctm}^2 \cdot d_0}\right)\right\}\frac{f_{ct}}{\gamma_v} bd \approx$$

$$\approx \left\{\zeta\left[0.88\frac{x}{d} + 0.02\right]\frac{b_{v,eff}}{b} + 0.015\frac{b_w}{b}\left(1 + \frac{1206}{d_0}\right)\right\}\frac{f_{ct}}{\gamma_v} bd =$$

$$\approx \left\{\zeta\left[0.88\frac{x}{d} + 0.02\right] b_{v,eff} + 0.015 b_w\left(1 + \frac{1206}{d_0}\right)\right\}\frac{f_{ct}}{\gamma_v} d =$$

For simplicity, and from the safe side, we assume $b_{v,eff} = b_w$:

$$V_{cu,min} \approx \left\{\zeta\left[0.88\frac{x}{d} + 0.02\right] + 0.015\left(1 + \frac{1206}{d_0}\right)\right\}\frac{f_{ct}}{\gamma_v} b_w d =$$

$$\approx \left\{\zeta 0.88\frac{x}{d} + 0.02\zeta + 0.015 + \frac{18}{d_0}\right\}\frac{f_{ct}}{\gamma_v} b_w d \approx$$

This expression is intended for the cases in which v_c is small compared to v_w. For this reason, x/d will be assumed to be equal to 0.2. Moreover, for further simplicity, the terms 0.02ζ and 0.015 are disregarded:

$$V_{cu,min} \approx \left\{\zeta 0.176 + \frac{18}{d_0}\right\}\frac{f_{ct}}{\gamma_v} b_w d \approx \; 0.18\left\{\zeta + \frac{100}{d_0}\right\}\frac{f_{ct}}{\gamma_v} b_w d$$

A3. Simplification of the expression for maximum shear strength, $V_{rd,max}$

For the maximum shear strength given by the concrete strut capacity, assuming $\alpha_{cw} = 1$ (no axial force), $z = 0.9$d, $v_1 = 0.6$ (conventional concrete), and cot $= 1.85$ (average value between reinforced and prestressed concrete beams according to the databases):

$$V_{Rd,max} = \alpha_{cw} b_w z v_1 f_{cd}\frac{cot\theta}{1 + cot^2\theta} = 1 \cdot b_w \cdot 0.9d \cdot 0.6 f_{cd}\frac{1{,}85}{1 + 1{,}85^2} \approx 0.225 f_{cd} b_w d$$

APPENDIX B: Derivation of LoA I from LoA II (CCCM)

B1. Simplification of the concrete contribution

From Loa II (CCCM):

$$V_{cu} = \zeta\frac{x}{d}\frac{f_{ct}}{\gamma_v} b_{v,eff} d$$

The size effect, assuming a/d = 4, becomes:

$$\zeta' = \frac{2}{\sqrt{1 + \frac{d_0}{200}}}\left(\frac{1}{4}\right)^{0.2} \approx \frac{1.5}{\sqrt{1 + \frac{d_0}{200}}}$$

Assuming now rectangular cross-section ($b_{v,eff} = b_w$), $\frac{x}{d} = 0.75\,(\alpha_e\,\rho_l)^{1/3}$ and $\alpha_e = 6.0$ (corresponding to $f_{ck} = 35$ MPa):

$$V_{cu} = \zeta'\frac{x}{d}\frac{f_{ct}}{\gamma_v} b_{v,eff} d = \zeta' \cdot 0.75(6 \cdot \rho_l)^{1/3}\frac{f_{ct}}{\gamma_v} b_{v,eff} d = 1.35\zeta'\rho_l^{1/3}\frac{f_{ct}}{\gamma_v} b_w d$$

B2. Detailed simplification of the shear reinforcement contribution:

$$V_{su} = 1.4(d_s - x)\cot\theta\frac{A_{sw}}{s} f_{ywd} = 1.4(d_s - x)\frac{0.85 d_s}{d_s - x}\frac{A_{sw}}{s} f_{ywd} \approx 1.20\frac{A_{sw}}{s} f_{ywd}$$